

UC Irvine

UC Irvine Electronic Theses and Dissertations

Title

Microfluidic Tools to Recapitulate the Tumor Microenvironment

Permalink

<https://escholarship.org/uc/item/36q2c8kj>

Author

Alonzo, Luis Fernando

Publication Date

2014

Peer reviewed|Thesis/dissertation

UNIVERSITY OF CALIFORNIA,
IRVINE

Microfluidic Tools to Recapitulate the Tumor Microenvironment

DISSERTATION

submitted in partial satisfaction of the requirements
for the degree of

DOCTOR OF PHILOSOPHY

in Biomedical Engineering

by

Luis Fernando Alonzo

Dissertation Committee:
Professor Steven C. George, Chair
Professor Abraham P. Lee
Professor Marian L. Waterman

2014

DEDICATION

To my family and friends in appreciation for their support.

TABLE OF CONTENTS

	Page
LIST OF FIGURES	v
LIST OF TABLES	vi
ACKNOWLEDGMENTS	vii
CURRICULUM VITAE	viii
ABSTRACT OF THE DISSERTATION	x
<i>CHAPTER 1 : Introduction</i>	<i>1</i>
1.1 Cancer – a leading cause of death	1
1.2 The hallmarks of cancer	2
1.3 The tumor microenvironment	3
1.3.1 Endothelial cells	5
1.3.2 Fibroblasts	6
1.4 Models of the tumor microenvironment	7
1.5 Our Approach	8
<i>CHAPTER 2 : Microfluidic device to culture 3D in vitro human capillary networks</i>	<i>9</i>
2.1 Abstract	9
2.2 Introduction	9
2.3 Materials	10
2.3.1 PDMS (polydimethylsiloxane) Microfluidic devices	10
2.3.2 Assembly of sealed devices	11
2.3.3 Cell Preparation	13
2.3.4 Hydrogel Preparation	14
2.4 Methods	15
2.4.1 Loading device	15
2.4.2 Introducing media into fluidic lines	16
2.4.3 Maintenance of culture within the microfluidic device	16
2.5 Notes	17
<i>CHAPTER 3 : Microfluidic device to study controlled interstitial flow mediated interactions between discrete multi-cellular environments</i>	<i>19</i>
3.1 Abstract	19
3.2 Introduction	20
3.3 Materials and Methods	22
3.3.1 Cell culture	22
3.3.2 Microfluidic device fabrication	23
3.3.3 Cell loading in microfluidic device	23

3.3.4 Finite element simulation	25
3.3.5 Verification of mass transport	26
3.3.6 Assessment of vessel network formation	26
3.3.7 Statistical analysis	27
3.4 Results and Discussion	27
3.4.1 Design and fabrication of the microfluidic based co-culture device	27
3.4.2 Theoretical and experimental validation of interstitial flow gradients	28
3.4.3 Interstitial flow mediates cellular communication in the vasculogenesis process	34
3.4.4 Potential applications and utility of the platform	35
<i>CHAPTER 4 : A Microfluidic Model of Tumor Cell Intravasation and Extravasation</i>	37
4.1 Introduction	37
4.2 Materials and Methods	38
4.2.1 Cell culture	38
4.2.2 Lentiviral transduction of tumor cells to constitutively express fluorescence	39
4.2.3 Microfluidic device fabrication	40
4.2.4 Cell loading in microfluidic device	41
4.2.5 Analysis of endothelial cell adhesion to PDMS surfaces	41
4.2.6 Quantification of vessel network formation	42
4.2.7 Assessment of tumor growth	42
4.2.8 Perfusion analyses and extravasation experiments	43
4.2.9 Statistical analysis	43
4.3 Results	44
4.3.1 Device construction for optimal vessel perfusion	44
4.3.2 ECFC-EC attachment to PDMS is dependent on non-competitive FN absorption	45
4.3.3 Platform to study intravascular tumor cell adhesion and “extravasation”	47
4.3.4 Platform to study tumor angiogenesis and intravasation	49
4.4 Discussion	51
REFERENCES	55

LIST OF FIGURES

	Page
FIGURE 1.1. THE TUMOR MICROENVIRONMENT	4
FIGURE 2.1. ASSEMBLY OF MICROFLUIDIC DEVICE FOR IN VITRO-PERFUSED HUMAN CAPILLARIES	12
FIGURE 2.2. MACROSCOPIC VIEW OF ASSEMBLED MICROFLUIDIC DEVICE	13
FIGURE 3.1. FOUR-CHAMBERED MICROFLUIDIC DEVICE TO STUDY INTERSTITIAL FLOW-DRIVEN COMMUNICATION BETWEEN DISCRETE MICROENVIRONMENTS	28
FIGURE 3.2. FINITE ELEMENT SIMULATIONS DEMONSTRATE CONTROL OF PRESSURE DISTRIBUTION AND ASSOCIATED INTERSTITIAL FLOW DISTRIBUTION WITHIN THE MICROFLUIDIC DEVICE	31
FIGURE 3.3. FLUORESCENCE RECOVERY AFTER PHOTBLEACHING (FRAP) VALIDATION OF SIMULATED INTERSTITIAL FLOW VELOCITY RESULTS.	33
FIGURE 3.4. FORMATION OF 3D <i>IN VITRO</i> INTERCONNECTED VESSEL NETWORKS IS DEPENDED ON INTERSTITIAL FLOW-DRIVED COMMUNICATION BETWEEN ECFC-ECS AND NHLFS.	35
FIGURE 3.5. TUMOR SPHEROID GROWTH AND MICROVESSEL NETWORK FORMATION IN FOUR-CHAMBERED MICROFLUIDIC DEVICE.	36
FIGURE 4.1 MICROFLUIDIC DEVICE USED TO SIMULATE TUMOR MICROENVIRONMENTS.	45
FIGURE 4.2 ECFC-EC ATTACHMENT ON MICROFLUIDIC ON MICROFLUIDIC CHANNEL MIMIC FUNCTIONAL ARTERIOLE AND VENUOLE COMPARTMENTS.	46
FIGURE 4.3. MICROFLUIDIC PLATFORM MAY BE USED TO MIMIC EXTRAVASATION EVENTS.	48
FIGURE 4.4. CONFOCAL IMAGING OF THE MICROTISSUE CONFIRMS ANASTOMOSIS.	49
FIGURE 4.5. ASSESSMENT OF VASCULAR PERFUSION IN THE VESSEL NETWORK WITHIN THE TUMOR MICROENVIRONMENT.	50
FIGURE 4.6. MICROFLUIDIC PLATFORM MAY BE USED TO MIMIC INTRAVASATION EVENTS.	51

LIST OF TABLES

	Page
TABLE 2.1. CELLULAR SEEDING DENSITY FOR DIFFERENT APPLICATIONS OF THE MICROFLUIDIC DEVICE.	14
TABLE 3.1 CELLULAR SEEDING PATTERN AND INTERSTITIAL FLOW EXPERIMENTAL CONDITIONS	25

ACKNOWLEDGMENTS

First and foremost, I would like to express my sincere gratitude to my advisor and committee chair, Professor Steven C. George, for his guidance and mentoring throughout my Ph.D. study and research. His enthusiasm and positive outlook were extremely helpful for the completion of this work.

I would also like to thank my committee members, Professor Abraham P. Lee and Professor Marian L. Waterman, for taking the time to share their expertise, helpful advice, and continuous support. Without their involvement, this dissertation would not have been possible.

Equally important was the contribution of the members of the George lab and the members of the UCI biomedical engineering department, as well as the Edwards Lifesciences Center for Cardiovascular Technology. Specially, Dr. Monica Moya, soon-to-be-doctor David Tran, Linda McCarthy, Anna Aleida, Sandra Lam, Yosuke Kurokawa, Lei Tian, Dr. Sean White, Dr. Claire Robertson, Dr. Seema Ehsan, Dr. Nicholas Merna, Dr. Venkatesh Shirure, Dr. Christopher Heylman, Zachary Campagna, Lisa Luevano, and Alexandra Crampton.

I would like to thank Springer Science + Business Media New York, LLC for their permission to include Chapter Two of my dissertation, which was originally published in *Biomimetics and Stem Cells: Methods and Protocols*.

Financial support throughout these five years was provided by the University of California, Irvine (UCI) Alliance for Graduate Education and the Professoriate (AGEP) Program, the department of Biomedical Engineering at UCI, the Ruth L. Kirschstein National Research Service Award for Individual Pre-doctoral Fellowships to Promote Diversity in Health Related Research (F31 CA163049-01) granted by the National Institute of Health (NIH), the Miguel Velez scholarship granted by UCI's graduate division, and the Public Impact fellowship granted by UCI's graduate division.

I would also like to mention my gratefulness to my family and friends. Their heartfelt support and encouragement furthered my motivation throughout this critical process.

Finally, I want to thank Anaid Yerena for her unconditional love and support. Words are not enough.

CURRICULUM VITAE

Luis Fernando Alonzo

EDUCATION

- Ph.D. Biomedical Engineering, University of California, Irvine (UCI), 2014
M.S. Biomedical Engineering, University of California, Irvine, 2011
B.S. Biomedical Engineering, *Cum Laude*, Florida International University (FIU), Miami, FL, 2008
Minor in Mathematics and Chemistry

EXPERIENCE

Research

- 2010 – Present **Cardiopulmonary Transport and Tissue Remodeling Lab, Irvine, CA**
Doctoral Candidate, NIH F31 Fellow – Advisor: Dr. Steven George
Developed a 3D microfluidic model of the tumor microenvironment to study the role of inflammatory signals on tumor progression and metastasis
- Jul – Sept 2012 **Laboratory of Lymphatic and Cancer Bioengineering, Lausanne, Switzerland**
Whitaker International Program Fellow – Advisor: Dr. Melody Swartz
Examined the interaction between tumor cells and lymphatic endothelial cells within custom made and commercially available interstitial flow *in vitro* models
- Apr – Jun 2010 **Biomolecular Microsystems and Nano Transducers Lab, Irvine, CA**
Graduate Rotational Student – Mentor: Dr. Abraham Lee
Constructed and monitored droplet fusion microfluidic devices based on the principle of Laplace pressures
- Jan – Mar 2010 **Cardiopulmonary Transport and Tissue Remodeling Lab, Irvine, CA**
Graduate Rotational Student – Mentor: Dr. Steven George
Established adequate qualitative measurements to assess cellular viability within a 3D microtissue using fluorescent spectroscopy
- Jul – Aug 2009 **Diffuse Optical Spectroscopic Imaging Lab, Irvine, CA**
AGEP Scholar – Mentors: Dr. Bruce Tromberg, and Dr. Albert Cerussi
Analyzed the theoretical light interaction within neonatal intestinal tissue for the aide in the diagnosis of Necrotizing Enterocolitis
- 2006 – 2008 **Laboratory of Vascular Physiology and Biotransport, Miami, FL**
Undergraduate Research Assistant – Mentor: Dr. Nikolaos Tsoukias
Performed experimental pressure myography studies on animal models to investigate the effect of nitric oxide on the regulation of vascular tone
- #### *Teaching*
- Mar – Jun 2011 **Biomechanics III (BME 110C), University of California, Irvine, CA**
Teaching Assistant

Professional

Jan – Jun 2009

Sintea Biotech LLC, Miami Beach, FL

Product Specialist

2007 – 2008

Oxylation, LLC, Miami, FL

Senior Design Project Researcher

PUBLICATIONS

Peer-Reviewed Journals

Alonzo, L. F., Moya M. L., Waterman, M. L., Lee, A. P., George, S. C. *3D in vitro Tumor Microtissues with Perfused Human Capillary Networks*. (In preparation)

Alonzo, L. F., Moya, M. L., Lee, A. P., George S. C. *Microfluidic Device to Study Controlled Interstitial Flow Interactions Between Discrete Multi-Cellular Environments*. (In preparation)

Tran, D. D., Lam, S., Simon M. G., **Alonzo, L. F.**, Lee, A. P., George, S. C. *Electrical Stimulation of iPSC-derived Cardiomyocytes in a 3D Tissue Matrix*. (In preparation)

Book Chapters

Moya, M. L., **Alonzo, L. F.**, and George, S. C. Microfluidic device to culture 3D in vitro Human Capillary Networks. *Methods Mol. Biol.* 2013 Oct 24. [PMID: 24155229]

ABSTRACT OF THE DISSERTATION

Microfluidic Tools to Recapitulate the Tumor Microenvironment

By

Luis Fernando Alonzo

Doctor of Philosophy in Biomedical Engineering

University of California, Irvine, 2014

Professor Steven C. George, Chair

Treatments for cancer remain elusive due, in large part, to the dynamic and unstable genome of most cancer cells. More recently it has become evident that tumor growth and progression to metastasis depends on the ability to recruit normal cells, such as endothelial cells, fibroblasts, as key accomplices. These observations suggest that selective targeting of normal cells, which have a stable genome, could be an effective alternative or complimentary approach in the overall management of the disease. Understanding of such relationship is key for the design of anti-metastatic therapeutics. However, much of the data reported in this field has been performed in xenograft models and/or 2D cultures; which are limited by the number of controllable variables, extrapolation to human tumor physiology, and not amenable for a high-throughput design. This work aims to address the role of the tumor microenvironment using a novel *in vitro* platform that combines microfluidic and tissue engineering technology to create a 3D tumor microarray in which the tumors receive their nutrients through perfused human microcirculation. This model is capable of replicating the physiology of the *in vivo*

tumor microenvironment; thus providing relevant physiological results. Most importantly, the impact of creating an *in vitro* 3D metastasis model with perfused human capillary bed could significantly enhance high-throughput anti-metastatic drug screening.

CHAPTER 1: Introduction

1.1 Cancer – a leading cause of death

Cancer is a family of diseases generally characterized by the uncontrollable growth of abnormal cells. Its history can be traced back to the ancient Egyptians in 3000 B.C., who recorded the first 8 cases of tumors or ulcers in breast tissue (1). These documents show the early attempts at treating the disease via cauterization of the affected area. Notably, these early assessments concluded that “no [effective] treatment”(1) could be found, giving us an early insight to the Egyptian’s awareness of the evasive and aggressive nature of the disease.

To this day, cancer remains a complex disease to treat. In 2008 alone, more than seven and a half million cancer-related deaths were reported worldwide, making it the leading cause of death for that year (2). In the United States, cancer is the second leading cause of death with more than half a million deaths annually (2), trailing only cardiovascular disease in annual mortality. Fortunately, recent trends show a decline in the mortality rates for both cancer and cardiovascular diseases in the U.S. by 11.9% and 30.8%, respectively (3). These promising statistical trends can be mainly attributed to improved therapeutics and modified living habits. However, more significant treatment advances in the cardiovascular field have decreased mortality by an order of magnitude, thus increasing the likelihood that cancer will soon become the leading cause of death in the U.S.

In 1971, President Nixon and Congress declared a “war on cancer.” Since then, the federal government has spent well over \$105 billion on the effort (4). Increased research

efforts and resources over the past 30 years have led to an even greater understanding of cancer. However, no consensus was achieved for a disease with noticeably diverse characteristics. The cancer research field was very broad and flooded with a collection of findings that proved difficult to place into a unifying theme or comprehensive understanding. It wasn't until the beginning of this millennium that a framework of cancer-specific traits was identified to better classify the general identity of all cancer variants (5). This guide, led by Douglas Hanahan and Robert Weinberg, intended to find the commonalities between all cancer cells as a means to focus the therapeutic development process and improve efficacy.

1.2 The hallmarks of cancer

In their revolutionary review article titled “Hallmarks of Cancer”, Hanahan and Weinberg identified six common traits that are representative of the malignant cancer cell population: “(i) self-sufficiency in growth signals, (ii) insensitivity to growth inhibitory (antigrowth) signals, (iii) evasion of programmed cell death (apoptosis), (iv) limitless replicative potential, (v) sustained angiogenesis, and (vi) tissue invasion and metastasis” (5). In 2011, Hanahan and Weinberg reviewed the progress of cancer research once again, a decade after the first set of hallmarks were published, and added two new hallmarks to the original list: “(vii) reprogramming of energy metabolism, and (viii) evading immune destruction” (6). Although some groups have disputed the uniqueness of these hallmarks to malignant cancer cells (7–9), they have mostly been enthusiastically accepted by the cancer research community (yielding a combined 17,519 citations as of August 2015) and have been instrumental in shaping our current understanding of the disease.

For the most part, mechanisms for these eight acquired traits have been explored from the reductionist point of view, which involves genetic and epigenetic alterations in the cancer cell. In line with this view, experimenting with monotypic cancer cells in isolation yielded a significant understanding of their components, inner workings, and behaviors. For example, many cancer cells have been shown to stimulate their own growth (first hallmark) through genetic variations that allow them to release autocrine growth factors (10), overexpress cell surface receptors (10–13), modify their interactions with the surrounding extracellular matrix (ECM) (14–16), and deregulate internal signaling pathways (17–21). However, growing evidence suggests that viewing cancer cells as autonomous entities within a tissue is far too simple, and does not take into consideration the contributions of the surrounding microenvironment. A closer look at the tumor stroma shows a heterotypic environment composed of normal cells (22–24). In the case of the first hallmark of cancer (example above), tumor-stroma interactions lead to the release of increased amounts of growth stimulating signals that enhance the tumor proliferative properties (5).

1.3 The tumor microenvironment

A novel way of depicting tumors recognizes them as highly complex organ systems (24). Normal healthy organs can be thought of as a collection of tissues that contain a diverse population of cells working synergistically to ensure proper behavior. These cells are generally compartmentalized within defined boundaries based on their function to ensure that their numbers and growth are controlled. Similarly, tumor tissues are composed of a heterogeneous and dynamically evolving microenvironment (Figure 1.1)

consisting of normal stromal cells, such as: endothelial cells, pericytes, fibroblasts, and various bone marrow-derived cells (22–26).

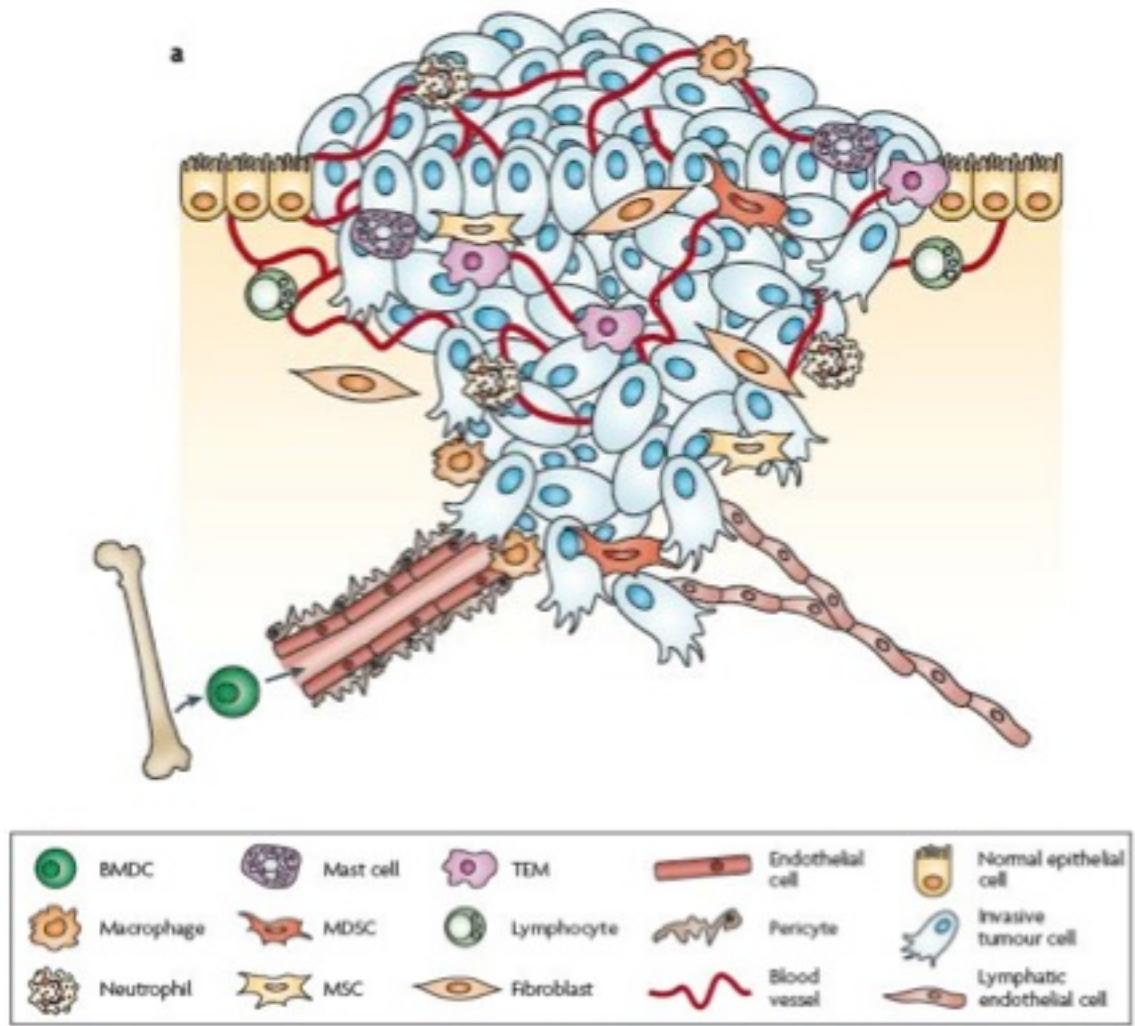


Figure 1.1. The tumor microenvironment. Adapted by permission from Macmillan Publishers Ltd: Nature Reviews Cancer (23), copyright 2009.

In benign tumors, these normal stromal cells act to suppress tumor growth and maintain organ stability. As tumor cells progress to malignancy via acquisition of the previously outlined hallmarks, a breach of the tissue’s architecture disrupts homeostasis. Once tissue homeostasis is lost, the stroma in the microenvironment becomes activated and can act to regulate and enhance all aspects of tumorigenicity (24, 27, 28). This altered

microenvironment may also contribute to the development of a resistance to anti-cancer treatment (29–32).

Within this vast and complex tumor microenvironment, there are two normal cell types that are most relevant to my work: endothelial cells and fibroblasts. These two cells are of particular importance due to their involvement in normal microcirculation functions. In the following, I focus on their reported roles in tumor growth and progression.

1.3.1 Endothelial cells

All normal tissues in the human body depend on blood supply for the delivery of vital nutrients and oxygen, as well as the removal of metabolic waste and carbon dioxide. A lining of adaptable endothelial cells -- flexible enough to adjust their numbers and arrangement to meet changing tissue needs -- makes up this essential vascular system (33). The formation of the blood vasculature *in vivo* can be achieved via two processes: vasculogenesis and angiogenesis. During early embryo development, and in some special cases during adulthood (34–36) vasculogenesis takes place, allowing *in situ* assembly of vessels from endothelial progenitor cells. Angiogenesis then follows through the growth of microvessel sprouts from existing blood vessels. A delicate balance of endogenous pro-angiogenic factors and inhibitors regulates both of these processes (37, 38).

Physiological vasculogenesis and angiogenesis are fundamental processes that occur during reproduction, development, and wound healing. Unfortunately, these processes may also play an active role in a variety of diseases, such as cancer. In fact, sustained angiogenesis is one of the aforementioned hallmarks of malignant tumors. Growth of tumor mass occurs in a progressive manner, initially relying on simple diffusion for the delivery of oxygen and nutrients, and removal of waste. In order to exceed the 1-2

mm limit of diffusion, the tumor cells activate and sustain an “angiogenic switch” that leads to the secretion of angiogenic factors (e.g. vascular endothelial growth factor, VEGF, angiopoietin, and fibroblast growth factor, FGF), loss of angiogenesis inhibitors (e.g. thrombospondin-1, endostatin), and the growth of microvessel sprouts from neighboring blood vessels (37, 39–42).

The newly formed vascular network is characteristically leaky and poorly organized (43–51). This leads to an increase of interstitial fluid pressure inside of the tumor mass, resulting in an inefficient delivery of blood to the affected area. Regardless of this fact, the tumor manages to regulate an adequate supply of nutrients. Most importantly, the vasculature allows the tumor mass to interact with surrounding cells that may be required for further survival and progression. For example, tumor cells can recruit tumor-associated macrophages (TAMs) through the release of soluble factors into the surrounding vasculature (e.g. colony stimulating factor-1, CSF-1). TAMs are believed to play a pivotal role in tumor metastasis through the release of soluble factors that promote further angiogenesis, tumor cell migration and intravasation (52).

1.3.2 Fibroblasts

The predominant cell type in normal tissue stroma is the fibroblast. Fibroblasts are primarily responsible for the production and maintenance of connective tissue components in the ECM, such as collagens, proteoglycans, proteolytic enzymes, inhibitors and growth factors (33, 53). In general, the fibroblast plays an important role in the support and repair of almost every tissue and organ. As such, they tend to be adaptable in their phenotype and function in order to meet specified needs (22, 23, 54). Fibroblasts appear to be the least specialized cells within the connective-tissue family, and display a great capacity to

differentiate into other cell types. In the context of angiogenesis, fibroblasts are recruited by endothelial cells within a mature vasculature to undergo differentiation into mural cells (e.g. pericytes and smooth muscle cells) and provide vessel stability (55–57).

In the tumor, activated fibroblasts have been referred to as “cancer associated fibroblasts” (CAFs) and exhibit a distinct phenotype characterized by higher proliferation, expression of α -smooth muscle actin (α -SMA), and are commonly surrounded by dense fibrillar collagens (53, 58). This particular phenotype has been linked to angiogenesis by guiding endothelial sprouts into the tumor mass. This vascularization process is associated with an abnormal increase of the release of pro-angiogenic factors, such as VEGF (59, 60). Thus, rather than fulfilling its normal stabilizing role, the activated fibroblasts render the tumor vessels leaky. Additionally, the CAF is associated with the recruitment of inflammatory cells and the restructuring of the ECM, which lead to further tumor invasion and intravasation.

1.4 Models of the tumor microenvironment

Much of the work investigating the underlying mechanisms of tumor growth and progression have been performed in xenotropic animal models (24, 61, 62). Similarly, the study of microcirculation during normal development or in pathology has also relied heavily on animal models. A brief review of the literature reveals an enormous range of models that have included several organ systems (e.g. brain, omentum, cheek pouch, dorsal skin fold chamber) and several animals species, including hamsters (63), rabbits (64), dogs (65), rodents (66, 67), and chick embryos (68). Each of the models has been created to address a specific question related to microcirculation processes such as tumor metastasis, inflammation/infection, or drug toxicity. The models are limited by the number of

controllable variables (e.g. flow, capillary density), extrapolation to human tumor physiology, and are not amenable for high-throughput design. Furthermore, a growing body of evidence demonstrates that cells, including tumor cells, display significant phenotype plasticity in 3D cultures relative to 2D cultures (or “flat biology”). More recently, the field of tissue engineering has provided glimpses of dynamic, controllable, and compelling 3D models of human physiology that could augment our understanding of tumor progression and metastasis.

1.5 Our Approach

This research was driven by the objective of creating a 3D *in vitro* system with perfused human capillaries to enhance the fundamental understanding of neovascularization, especially in relation to tumor progression and metastasis. To achieve this goal we have constructed a microtissue, combining microfabrication techniques with a cellular 3D culture. This dissertation begins by describing the protocol employed to create the microfluidic device with perfused human capillary networks and discusses its potential applications for tissue specific purposes (Chapter 2). Applying these principles, we then focus on adapting the microfluidic device to improve our understanding of the effect of interstitial flow on heterocellular communication, with a focus on neovascularization (Chapter 3). Finally, we create a “tumor-on-a-chip” device with perfused capillary networks and interstitial flow in order to model the various steps of the metastatic process (Chapter 4).

CHAPTER 2: Microfluidic device to culture 3D in vitro human capillary networks

2.1 Abstract

Models that aim to recapitulate the dynamic *in vivo* features of microcirculation are crucial for studying vascularization. Cells *in vivo* sense not only biochemical cues (e.g. growth factor gradients) but also mechanical cues (e.g. interstitial flow, vessel perfusion). Integrating the responses of cells, the stroma and the circulation in a dynamic 3D setting will create an environment suitable for the exploration of fundamental vascularization processes. Here in this chapter, we describe an *in vivo* inspired microenvironment that is conducive to the development of perfused human capillaries.

2.2 Introduction

Understanding the mechanisms that regulate vascularization is essential for the development of tissue engineering strategies. Our current understanding of the vascularization process has primarily relied on 2D and 3D co-culture *in vitro* models, as well as *in vivo* animal models. From these model we have gained significant knowledge about fundamental cellular interactions between the primary components of vascular structures, endothelial cells, and the surrounding stromal cells (i.e. fibroblasts, pericytes, smooth muscle cells), which guide vascular development and maturation via paracrine signaling and physical contact (69, 70). Many of these systems, however, lack the complexity needed to mimic dynamic *in vivo* microenvironment parameters such as interstitial flow and vessel perfusion. To address these limitations, various research groups have explored the use of microfluidic technologies in order to create controllable, dynamic

in vivo-like environments (71–76). These platforms have the potential to recreate relevant environmental cues (e.g. cell-cell communications, growth factor gradients, and interstitial flow) while maintaining flexible and convenient culture conditions (e.g. high-throughput, and real-time imaging).

Here we describe a microfluidic-based system that allows for real-time visualization of perfused human capillary networks in a dynamic microenvironment that includes interstitial flow. In this system, endothelial cells and stromal cells are allowed to self-assemble in a 3D matrix that is conducive for the development of perfused human capillaries, achieving flows within the physiological range (71). This platform can be used to study the roles of interstitial flow (73), heterotypic and homotypic cell interactions, and growth factors during the development of *in vitro* human capillary networks. In addition, this platform is easily adapted to include tissue specific functions (e.g., cardiac muscle) as well as models of disease that involve microcirculation.

2.3 Materials

Below is a detailed description of the methods employed to create the perfused capillaries and microfluidic device.

2.3.1 PDMS (polydimethylsiloxane) Microfluidic devices

1. Prepare PDMS by mixing the cross-linker, Sylgard 184, with the curing agent (Dow Corning) at a ratio of 10:1. For example, 10 grams of PDMS are cured with 1 g of curing agent. Ensure that the curing agent and cross-linker are well mixed.
2. De-gas mixture in a vacuum chamber for 30 minutes to remove excess air bubbles from solution.

3. After 30 minutes, solution should be essentially bubble-free and can then be poured onto an SU-8 patterned microfluidic casting mold (approximately 20-25g). Note that details on how to create a SU-8 mold are not included in this report, but can be found in a variety of additional studies (77, 78).
4. Place the SU-8 mold coated with the PDMS solution in the vacuum chamber for an additional 15 minutes to remove any further air bubbles.
5. Place the mold with PDMS into an oven at 65°C and allow it to cure for at least 8 hours (and no more than 2 days) prior to removing it from mold.

2.3.2 Assembly of sealed devices

1. Carefully remove the PDMS device from the mold using a surgical blade to cut around the perimeter of the device. Carefully lift off the mold. (*see Note 1*)
2. Using a 16G needle, punch both the inlet and outlet of the tissue chambers and the microfluidic lines into the device. Using a nitrogen air gun, blow away any excess debris from the device surface. (*see Note 2*)
3. For 3.5 minutes, plasma treat all three pieces that make up the microfluidic device: glass slide/cover glass, a separate thin sheet of PDMS (thickness 500-750 μm), and a PDMS piece with a negative replica of mold design.

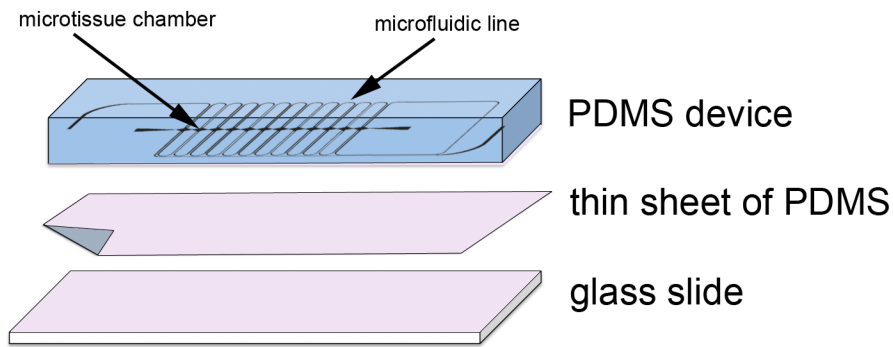


Figure 2.1. Assembly of microfluidic device for in vitro-perfused human capillaries. Plasma-treated surfaces (Indicated in pink color) of PDMS device, sheet of PDMS, and glass slide are bonded together and baked in 120°C oven for 15 mins to obtain PDMS-enclosed chambers.

4. Bond all three plasma treated pieces to each other quickly (< 90 seconds) to seal the microfluidic device. The PDMS piece representing the negative replica of the mold design should be facing up and be bonded to the thin sheet of PDMS. The glass slide-treated surface is then bonded to thin sheet of PDMS. (*see Note 3*) (Figure 1)
5. Place the bonded device in a 120°C oven for 15 minutes.
6. Bond glass vials (i.e. media reservoirs) to the inlet/outlet holes of the assembled microfluidic device using a mixture of PDMS. To prevent PDMS from seeping into the inlet/outlet holes, place pipette tips on all inlet/outlet holes of the device.
7. Dip the bottom of the pre-cut glass vials into the PDMS mixture and place through the pipette tip onto the top surface of the device.
8. Place the completely assembled device in a 65°C oven overnight to cure.
9. Sterilize the assembled PDMS device (Figure 2) in an autoclave

2.3.3 Cell Preparation

1. Trypsinize, collect, and count the cells needed for the experiment.
2. Reconstitute cells at the desired cell density (see Table 2.1) and combine them.

Cells can then be spun down together. Note that cord blood endothelial colonies forming cell-derived endothelial cells (ECFC-EC) and normal human lung fibroblasts (NHLF) work well for this assay. However, other endothelial cell sources (e.g., human umbilical vein endothelial cells, HUVEC) and stromal cell sources (e.g., dermal fibroblast) have also been successfully substituted (79–81).

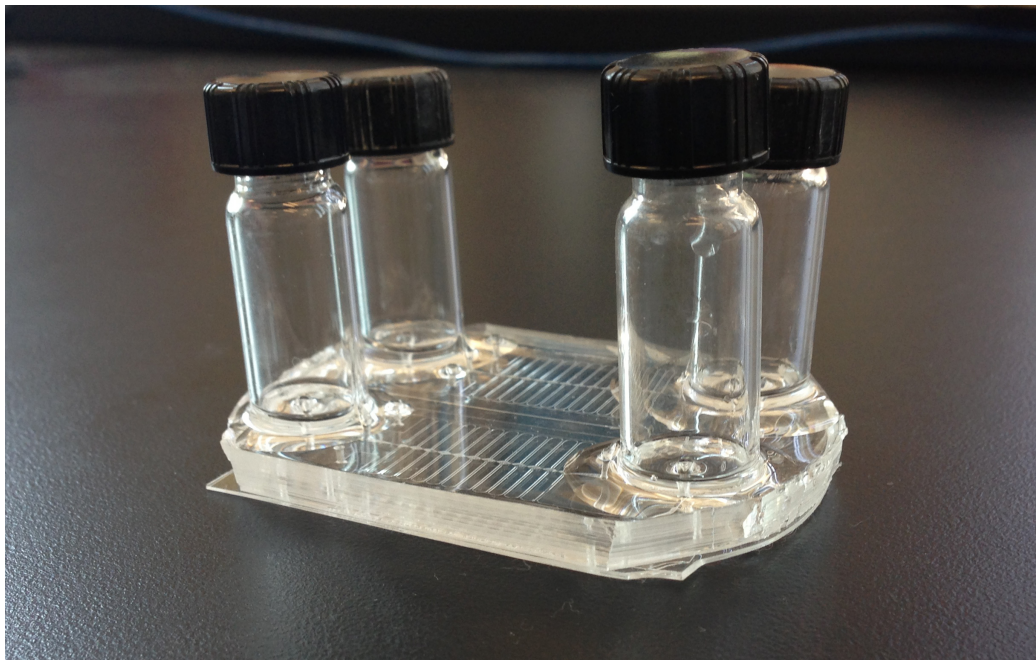


Figure 2.2. Macroscopic view of assembled microfluidic device. Glass vial reservoirs are attached to the PDMS chamber bonded to a thin layer of PDMS and a glass slide. Also visible are the microfluidic lines that will contain cell culture media or fibrin and cells.

Experiment	Cells Density
<i>Vasculogenesis model</i>	
ECFC-ECs	2.5 x 10 ⁶ cells/ml
NHLFs	5 x 10 ⁶ cells/ml
<i>Tumor vasculogenesis model</i>	
SW620s	160,000 cells/ml
ECFC-ECs	2.5 x 10 ⁶ cells/ml
NHLFs	5 x 10 ⁶ cells/ml

Table 2.1. Cellular seeding density for different applications of the microfluidic device.

2.3.4 Hydrogel Preparation

1. Prepare fibrinogen (Sigma) by reconstituting it in Dulbecco's Phosphate Buffered Saline (DPBS) to a final concentration of 10 mg/ml
2. Allow the fibrinogen solution to warm and dissolve by placing it in a 37°C water bath for a minimum of 15 minutes.
3. Once the fibrinogen solution is fully dissolved, the solution should then be sterile filtered using a 0.22µm syringe filter

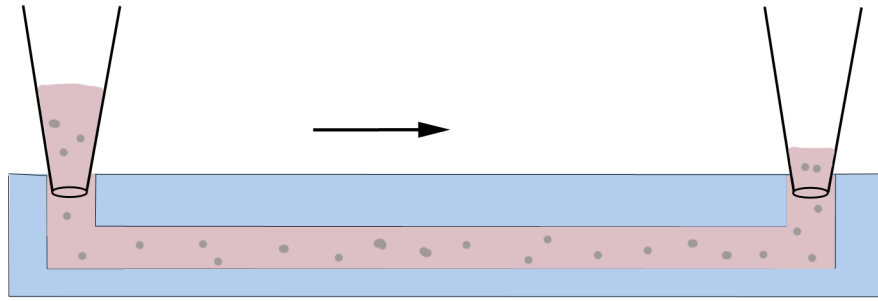


Figure 2.3. Side-view schematic of loading tissue chambers. Prior to polymerization, the fibrinogen-cell mixture is micropipetted into the inlet of the tissue chamber using steady even pressure.

2.4 Methods

2.4.1 Loading device

1. Remove devices from the autoclave and allow them to cool at room temperature before loading them with hydrogel and cells.
2. Resuspend cells in prepared fibrinogen according to the desired volume and cell density (*See Note 4*)
3. Pipette 30 μ l of cell-fibrinogen mixture into a microcentrifuge tube containing 1.8 μ l of 50 U/ml thrombin and mix thoroughly, while avoiding the creation of air bubbles. (*See Note 5*)
4. Using a filtered pipette tip, quickly (in less than 3 minutes) collect a minimum of 25 μ l of the mixture and insert it into the inlet of the tissue channel by applying steady and even pressure to avoid leakage of the hydrogel into adjacent fluidic channels. Keep applying a steady pressure until the mixture reaches the outlet of the tissue chamber. (Figure 3) (*See Note 6*)
5. Incubate device in a 37°C humidified incubator for a minimum of 30 minutes and a maximum of one hour to ensure full fibrin polymerization.

2.4.2 Introducing media into fluidic lines

1. Insert 200 μ l of fully supplemented EGM-2 (Lonza) into the inlet of one adjacent microfluidic channel by applying steady, even pressure until the media reaches the outlet of the microfluidic channel forming a small droplet of media.
2. For the other microfluidic line, insert into a small piece of tygon tubing (0.02" ID x 0.06" OD) to the outlet to connect or couple the two microfluidic lines. Repeat this step with the second channel to ensure that the media enters and forms a small droplet of fluid at the end of the microfluidic line. Alternatively, the microfluidic lines may remain uncoupled, if desired, by not employing the small plastic tubing.
3. Connect fluid-filled tubing with the outlet of the first channel and avoid introducing any air gaps. (*See Note 7*)
4. Once connected, fill reservoirs with media. Set a height difference of 10 mm between the two reservoirs to allow media to flow through the fluidic channels as well as across the tissue chambers. Note that a larger or smaller height difference can be employed to produce higher or lower flows, respectively, if desired.
5. Place assembled device into a 20% O₂ incubator overnight.

2.4.3 Maintenance of culture within the microfluidic device

1. The day after seeding the device, replace the media with EGM-2 without VEGF and bFGF. The device can then be moved to a 5% O₂ incubator for the remainder of the study, if desired. (*See Note 8*)

2. Continue to level the fluid in the reservoir every other day to maintain the 10 mm (or other) height difference.
3. After 7 days of culture, reverse the direction of the interstitial flow across the tissue chamber by reversing the pressure head in the reservoirs. This encourages vessels to grow towards both pores on either side, and to form connections with the microfluidic channels.

2.5 Notes

1. For easy removal of the PDMS mold from the wafer mold, silanize the wafer prior to casting.
2. If bubbles occur between the layers of PDMS, use a flat-edged surface to press bubbles away from chambers or microfluidic lines. Bubbles in between layers that are away from chambers or microfluidic line are not a problem as they don't interfere with the loading of the device.
3. Use scotch tape on the surfaces of the device to remove stubborn debris from the PDMS.
4. Aliquot cell mixtures in smaller sets for loading to avoid premature polymerization of the hydrogel. For example if loading 8 samples, split cells into 2 sets of 4 loadings.
5. The fibrinogen-cell mixture will begin polymerizing quickly upon adding thrombin, so perform this step quickly to avoid damaging the gel or creating uneven polymerization.
6. To avoid introducing bubbles into the cell-fibrinogen-thrombin mixture, change tips in between mixing the solution and loading the solution into the device.

7. When connecting tubing and microfluidic channels make sure to touch the liquid droplet at the microfluidic line outlet to the small droplet formed at the tip of the tubing so as to always maintain fluid-fluid contact and avoid introducing air bubbles.
8. To minimize evaporation of media from the reservoirs of the device while in the incubator, create a secondary humidity chamber by placing the microfluidic devices into a box with a non air tight lid containing a reservoir of about 20ml of water.

CHAPTER 3: Microfluidic device to study controlled interstitial flow mediated interactions between discrete multi-cellular environments

3.1 Abstract

Understanding the process of vascularization is key for developing therapeutic and regenerative therapies. Models of microcirculation that aim to recapitulate dynamic *in vivo* features, such as interstitial flow and vessel perfusion, are crucial for studying vascularization processes. While endothelial cells are the key players in the vascularization process and have been the primary focus of angiogenesis research, the activation of the fibroblast in the surrounding matrix provides important cues for the organization of the endothelial cells. This study examines the role of stromal cells in vessel network formation using a novel 4-chambered device that allows for the visualization of the steps of vessel network assembly and angiogenic sprouting in a dynamic microenvironment with interstitial flow. In this device the vessel network can self assemble (vasculogenic-like process) and extend into a second compartment via angiogenesis without exogenous VEGF or bFGF medium supplementation. Interstitial flow and the direct contact of NHLFs with ECs both affected the formation of the network. Current ongoing work is focused on further characterization of the vessel network and investigating the molecular mechanism governing the interplay between NHLFs and ECs.

3.2 Introduction

Traditionally, a reductionist approach has been used to study cellular fate and function. Experimenting with monotypic cells in isolation has yielded a great understanding of their components, inner working, and behavior. This view, however, ignores the significant role of the cellular microenvironment. Cells within a tissue experience a combination of biological, chemical, and mechanical cues originating from their surroundings (e.g. , cell-cell contact, soluble factors, interstitial fluid forces), which largely influence their response.

While we have gained valuable insights about how cells behave within two dimensional (2D) *in vitro* culture systems, it is now well accepted that three-dimensional (3D) *in vitro* cultures can better mimic *in vivo* conditions. In fact, cells have been shown to behave differently and employ alternate pathways when cultured in 3D (61, 82–84). Embedding cells within an extracellular matrix (ECM) – either naturally derived or synthetic – is a common technique used to accomplish this task. This technique has been shown to provide the biomechanical and biochemical cues that cells experience *in vivo*, which in turn affect cellular phenotype, growth, and migration (85–87). These 3D methods possess tunable parameters (e.g. matrix density, stiffness, binding domains, protein composition) that have yielded contributions being studied in tumor development and capillary morphogenesis, among other cellular activities.

The heterotypic diversity of the cellular microenvironment has also been well characterized. Cells do not live in isolation within this vast ECM; in reality, they share and interact with a variety of cells in their vicinity through either direct contact or paracrine signaling with distant cells. For example, capillary morphogenesis has been shown to be

dependent on the interplay between endothelial cells and stromal cells (e.g. fibroblasts, pericytes, mesenchymal stem cells) (57, 88–90). The tumor microenvironment is another excellent example. While much attention has been given to the genetic and epigenetic mutations of tumor cells, recent efforts have been focused on the surrounding “normal” cells (e.g. endothelial cells, cancer associated fibroblasts, infiltrating immune cells) (22–26), which together play a pivotal role in various stages of tumor progression and metastasis.

Mechanical forces in the cellular microenvironment, such as interstitial flow, are also responsible for modulating cellular behavior. Interstitial flow can distinctly impact extracellular gradients of solutes, enhance transport of nutrients and waste, and significantly influence several morphogenic processes (e.g., vasculogenesis and lymphangiogenesis) (91–93). Physiological interstitial flow has been shown to be in the range of 0.1-2 $\mu\text{m/s}$ (94); however, we have previously shown that super and sub physiological ranges *in vitro* have driven vascular network formation (71, 73). Pathological conditions, such as cancer, experience characteristically abnormal interstitial flows, which play a significant role in tumor progression, migration, and drug resistance (95–97).

Current *in vitro* systems fall short in incorporating these three *in vivo*-like parameters: 3D microenvironment, heterotypic cellular composition, and interstitial fluid forces. Many variations of the Boyden chamber have been traditionally used to examine heterocellular interactions, but most of these studies still involve 2D culturing conditions (98). A number of recent studies have modified the Boyden chamber assay to incorporate 3D gels (99). These systems are generally easy to use, but do not allow cell behavior to be monitored as a function of time, and do not provide well-defined concentration gradients.

In this research, we have developed a novel microfluidic device that allows for precise control of spatial-temporal interactions between adjacent heterotypic cellular environments. The communication ports, a special feature of the device, have been specifically designed to control the loading of two discrete interconnected 3D cell-containing hydrogels. In addition, hydrostatic pressure forces can be arranged across the three-dimensional tissues to create diverse interstitial flow patterns, which can lead to on demand endogenous and/or exogenous soluble factor gradients. We anticipate that this platform could be used as an essential tool to study the effects of directional interstitial flow and heterocellular communication in many important physiological and pathological processes (e.g. angiogenesis and tumor progression). As an endpoint, we have chosen to investigate the role of these relevant mediators of cellular behavior on the biological process of vasculogenesis.

3.3 Materials and Methods

3.3.1 Cell culture

Human Endothelial Colony Forming Cells – Endothelial Cells (ECFC-ECs) were derived from cord blood as previously described by our lab (81) and expanded on 1% gelatin-coated flasks in endothelial growth medium-2 (EGM-2; Lonza, Wakersfield, MD). ECFC-ECs were used at passages 4-6 during the experiments. Commercially available normal lung human fibroblasts (NHLFs; Lonza) were grown in fibroblast growth media (FGM; Lonza) and were used at passages 5-7. All cells were cultured in a humidified incubator at 37°C, 5% CO₂, and 20% O₂ prior to their introduction to the 4-chambered microfluidic device.

3.3.2 Microfluidic device fabrication

Standard soft lithography and replica molding processes were utilized to fabricate the 4-chambered microfluidic device. A master mold was created via the ultraviolet patterning of a 100 μm thick photoresist, SU-8 (MicroChem, Newton, MA), on a silicon wafer. A polydimethylsiloxane (PDMS; Dow Corning, Elizabethtown, KY) mixture composed of 10:1 (w/w) base to curing agent was poured over the master mold and thermally cured at 65°C overnight. Once fully cured, the PDMS was cut and peeled off the mold; leaving a negative imprint of the 4-chambered design pattern. Inlet and outlet holes were punched onto the PDMS piece to allow for introduction of the extracellular matrices and injection of cell culture media. All debris was removed from the PDMS piece, followed by oxygen plasma treatment for 3.5 mins at 250 mTorr. A 500-750 μm thick PDMS sheet and a 130-170 μm thick glass coverslip (Thermo Fisher Scientific, Waltham, MA) were simultaneously plasma treated and covalently bonded to the PDMS piece to seal its channels and provide mechanical support, respectively. The completed device was then baked at 120°C for a few minutes to invert the hydrophilic properties acquired during the plasma treatment process. To sterilize and prepare the device for cell culturing, the device was autoclaved at 120°C prior to the experiment.

3.3.3 Cell loading in microfluidic device

For tissue preparation, cells were trypsinized and resuspended in 10 mg/ml bovine fibrinogen (Sigma-Aldrich, St. Louis, MO) dissolved in 1x Dulbecco's Phosphate Buffered Saline (DPBS; Gibco). Four different cellular conditions were mixed with the fibrinogen solution (Table 3.1) at a final concentration of 2.5×10^6 ECFC-ECs/mL in ECFC-EC containing conditions, and 5.0×10^6 NHLFs/mL in NHLF containing conditions. Thrombin

(Sigma-Aldrich) was added to the cell-fibrinogen mixture to produce a final concentration of 3 U/mL to begin the gel polymerization process, and the mixture was pipetted quickly into the tissue compartments. Each one of the two tissue compartments was carefully loaded in a sequential order and the device was then incubated at 37°C for 1 hr to finalize the fibrin polymerization. The media was then pipetted into the fluidic lines adjacent to each of the tissue compartments. The volume of each pipette tip was adjusted in order to create a pressure gradient across the tissue, and the microfluidic platform was placed in a 20% O₂ incubator for 7 days. Media volumes were replaced and readjusted every 24 hours to maintain the desired pressure drop across the tissue for the duration of the experiment.

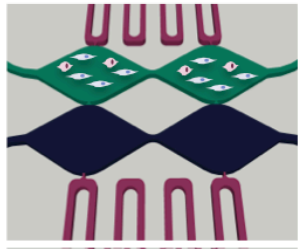


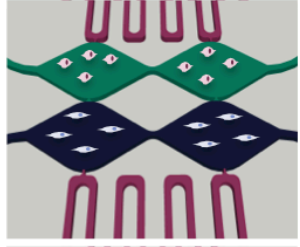


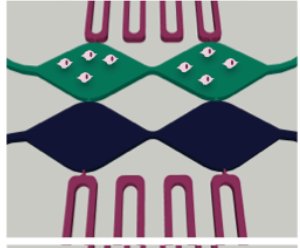


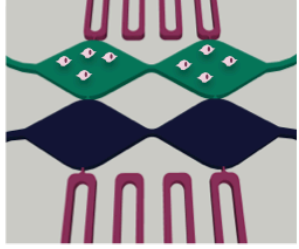


		Cellular Patterning	Interstitial Flow (ΔP)
Condition 1		Top: ECFC/NHLF	 Transverse
		Bottom: Acellular	 Longitudinal
Condition 2		Top: ECFC	 Transverse
		Bottom: NHLF	 Longitudinal
Condition 3		Top: ECFC	 Transverse
		Bottom: Acellular	 Longitudinal
Condition 4		Top: ECFC	 Transverse
		Bottom: Acellular +NHLF conditioned media	 Longitudinal

Table 3.1. Cellular seeding pattern and interstitial flow experimental conditions.

3.3.4 Finite element simulation

The experimental fluid flow conditions were simulated using COMSOL Multiphysics® 3.5a (Burlington, MA). A computer-aided design (CAD) model of the 4-chambered microfluidic device was constructed and solved by a two-dimensional steady state analysis of the incompressible Navier-Stokes equation. All surfaces, except the inlet and outlet, were set to be have a no-slip boundary condition. Other initial conditions specified in the simulation were: the dynamic viscosity of water (0.748 mPa.s), the density

of water (1 kg/m^3), the porosity of fibrin gel (0.99), and the permeability of fibrin gel ($1.5 \times 10^{-13} \text{ m}^2$). The resulting pressure and velocity field simulations were used to interpret the magnitude and pattern of convection.

3.3.5 Verification of mass transport

Fluorescent recovery after photobleaching (FRAP) technique was used to measure the flow across the fibrin gel using a modified protocol (100, 101). Both of the tissue compartments of the 4-chambered microfluidic device were loaded with a 10 mg/ml fibrin gel in the absence of cells. FITC-dextran (70 kDa, Sigma-Aldrich) was added to the adjacent fluidic lines via pipette tips. Volumes of the FITC-dextran containing solution were then readjusted to achieve the two distinct interstitial flow profiles modeled in COMSOL. FRAP was then performed on the device, at the junctions connecting each tissue chamber, using a confocal microscope (Zeiss LSM 700, Carl Zeiss AG, Feldbach, Switzerland). A circular region of $30 \text{ }\mu\text{m}$ was bleached, and images were taken every second for a total of 30 seconds.

3.3.6 Assessment of vessel network formation

After 7 days of culturing, the microtissues within the 4-chambered microfluidic device were subjected to immunofluorescent staining with CD31-antibodies using a modified staining protocol (71, 81). The microtissues were initially fixed in 10% formalin that was introduced through the adjacent fluidic channels for 18 hrs. The staining process consisted of exposing the microtissues to mouse anti-human CD31 antibody (Dako, Carpinteria, CA) for 1-2 days, followed by Alexa-Fluor 488-conjugated goat anti-mouse IgG (Invitrogen, Grand Island, NY) for an additional 1-2 days. Images of the stained

microvessels were taken using an inverted fluorescence microscope (Olympus IX83, Central Valley, PA). Vessels stained positive for CD31 were analyzed using AngioTool (102), a software for quantitative assessment of various vessel parameters.

3.3.7 Statistical analysis

Statistical analyses were performed using one-way analysis of variance (ANOVA) with StatPlus (AnalystSoft Software). Comparisons between groups were made with the Student's t-test for multiple comparisons. All data are presented as the mean \pm standard deviation. Results are statistically significant for $p < 0.05$.

3.4 Results and Discussion

3.4.1 Design and fabrication of the microfluidic based co-culture device

Using standard PDMS micro-molding, we constructed a microfluidic device that consists of two discrete tissue channels (green and blue channels, Figure 3.1B)– each containing two daisy-chained mm-sized chambers (1×2 mm) that connected in series. The two tissue channels were loaded separately with cell-containing hydrogels resulting in the two daisy-chained chambers containing a homotypic cellular composition. In turn, the two tissue channels were interconnected in parallel through two $30 \mu\text{m}$ wide and $100 \mu\text{m}$ high pores. These micropores are specifically designed to mimic a capillary burst valve (71, 73, 103), which aids in the patterning of each hydrogel after it is sequentially loaded within the device. In short, successful containment of the gels at the connecting micropores is dependent on the surface tension of the leading edge, which matches and opposes the driving hydrostatic pressure produced when loading. As this occurs, the hydrogel stops flowing and is retained within its designated microfluidic channel. Figure 3.2C shows two

distinct fibrin gels (TRITC and FITC labeled) that, when sequentially loaded, result in a continuous 3D environment between the two tissue compartments.

In addition, on either side of the 4-chambered region that houses the 3D cellular microenvironments, two fluid-filled microchannels are connected via two pores following the same geometry of the previously described capillary burst valve. The microfluidic channels serve to provide a dynamic supply of media to the tissue-containing region, which is controlled through hydrostatic pressure gradients that are achieved by adjusting the media heights in the associated pipette tips.

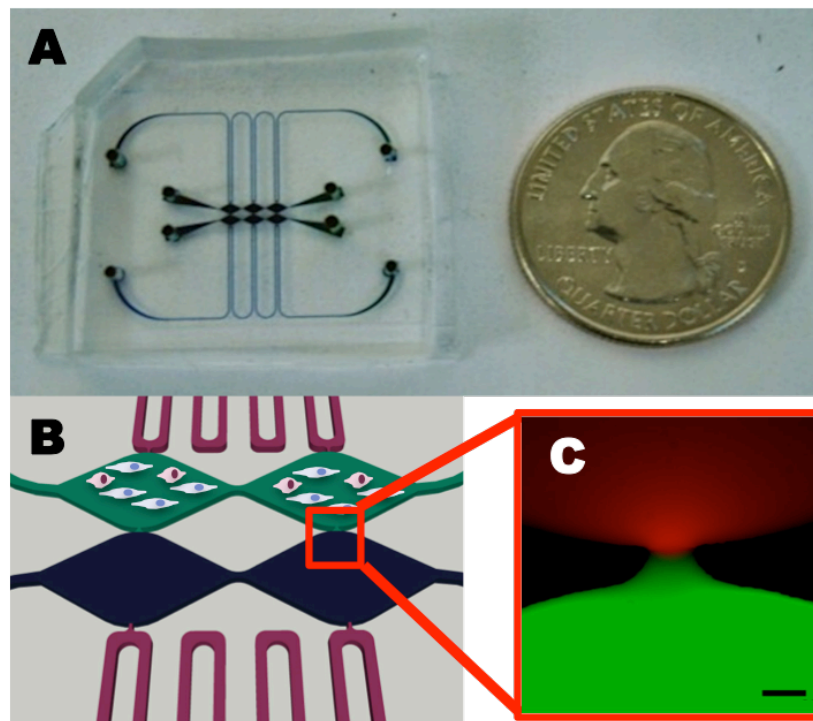


Figure 3.1. Four-chambered microfluidic device to study interstitial flow-driven communication between discrete microenvironments.

3.4.2 Theoretical and experimental validation of interstitial flow gradients

Even though physiological interstitial velocities are relatively low (94), the role of convection in the overall distribution of solutes can be significant. For example, cell

response has been reported to be influenced by morphogen gradients as low as 1% across a cell (104). Through the control of hydrostatic pressure (ΔP) and the design of the microfluidic channels, our device is able to recreate a controlled cellular microenvironment where these effects can be studied in detail. We studied two different interstitial flow configurations: one was set up to allow communication between the chambers in series (longitudinal), and the second was set up to allow for communication between the channels in parallel (transverse).

To create a longitudinal interstitial flow pattern (x-direction), the design of the fluid-filled microchannels employs a serpentine configuration. This configuration offers an increased resistance to media flow between the two pore connections in order to manipulate the pressure across the tissue chamber and, thus, mass transport within the 4-chambered region. In this configuration, the pattern of the media flow is achieved across the tissue chambers in series, by having high pressure on the left side (α and β) of the tissue chamber and low pressure on the right side (α' and β'). The transverse flow configuration is set up to allow media flow across the tissue chambers in parallel to span from the bottom tissue chamber (Figure 3.2B – blue channel) up to the top tissue chamber (Figure 3.2B – green channel), by having high pressure on the top side (α and α') and low pressure on the bottom side (β and β').

Finite element simulations were performed using a COMSOL Multiphysics® 3.5a model to predict the pressures within the hydrogel 4-chambered microtissue and resulting interstitial flow velocity in the absence of cells (Figure 3.2). To simulate a longitudinal interstitial flow pattern, a ΔP of 20 mmH₂O was applied from α to β , as well as α' and β' (Figure 3.2A). From the pressure simulations, a linear drop can be observed within the

tissue chamber from the high entrance pressure on the left to the low exit pressure on the right. The simulated streamlines (Figure 3.2B) demonstrate that flow is predominantly in the longitudinal direction (x-axis) with no significant interaction between the parallel chambers. It is important to note that the design of the two discrete tissue channels includes a region where the area is reduced to 60 μm . This geometrical configuration allows for an acceleration of the interstitial fluid, which enhances the convective communication between the two chambers in series.

Alternatively, to simulate a transverse interstitial convective flow pattern, a ΔP of 20 mmH₂O was applied from α to α' , as well as β to β' (Figure 3.2C). Similarly, the pressure drop simulation shows a linear drop within the tissue chamber from the high entrance pressure on the top side to the low exit pressure on the bottom side. The simulated streamlines (Figure 3.2D) demonstrate that flow is predominantly in the transverse direction (y-axis) with no significant interaction between the chambers in series. The aforementioned narrowing of the chambers in series also plays a significant role in this configuration, as it limits the diffusion of soluble factors in the direction perpendicular to the overall interstitial flow direction.

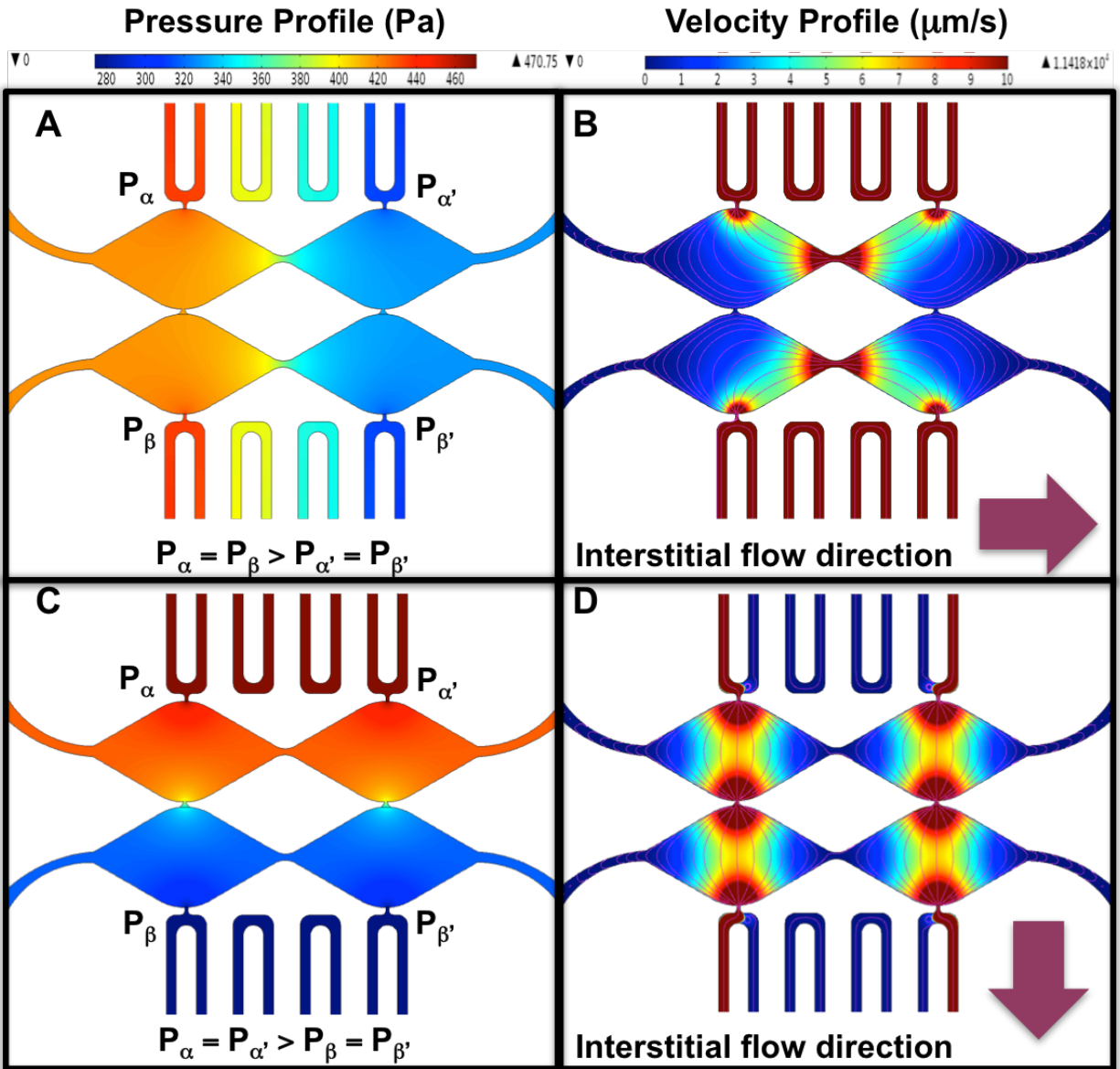


Figure 3.2. Finite element simulations demonstrate control of pressure distribution and associated interstitial flow distribution within the microfluidic device.

Fluorescence recovery after photobleaching (FRAP) has been widely used to study the mobility of macromolecules in various mediums and tissues (100, 105). We surveyed two regions of the device to validate our finite element simulation flow velocity results: 1) the tapering pore between the tissue chamber in series, and 2) the connecting pore between the top and bottom tissue chambers in parallel (Figure 3.3A). These two regions

are of particular significance due to our simulation that the most extreme interstitial flow velocities occurred herein these regions. After generating a pressure gradient that produced a longitudinal direction of flow, the fluid flow velocity within the fibrin gel was $69 \mu\text{m/s}$ at the first spot surveyed (Figure 3.3B), while the velocity was negligible in the connection between the chambers in parallel. Alternatively, when a transverse pressure gradient was applied, the measured fluid flow velocity within the fibrin gel was $8 \mu\text{m/s}$ at the pore between the chambers in parallel, while it was negligible in the tapering geometry between the two chambers in series.

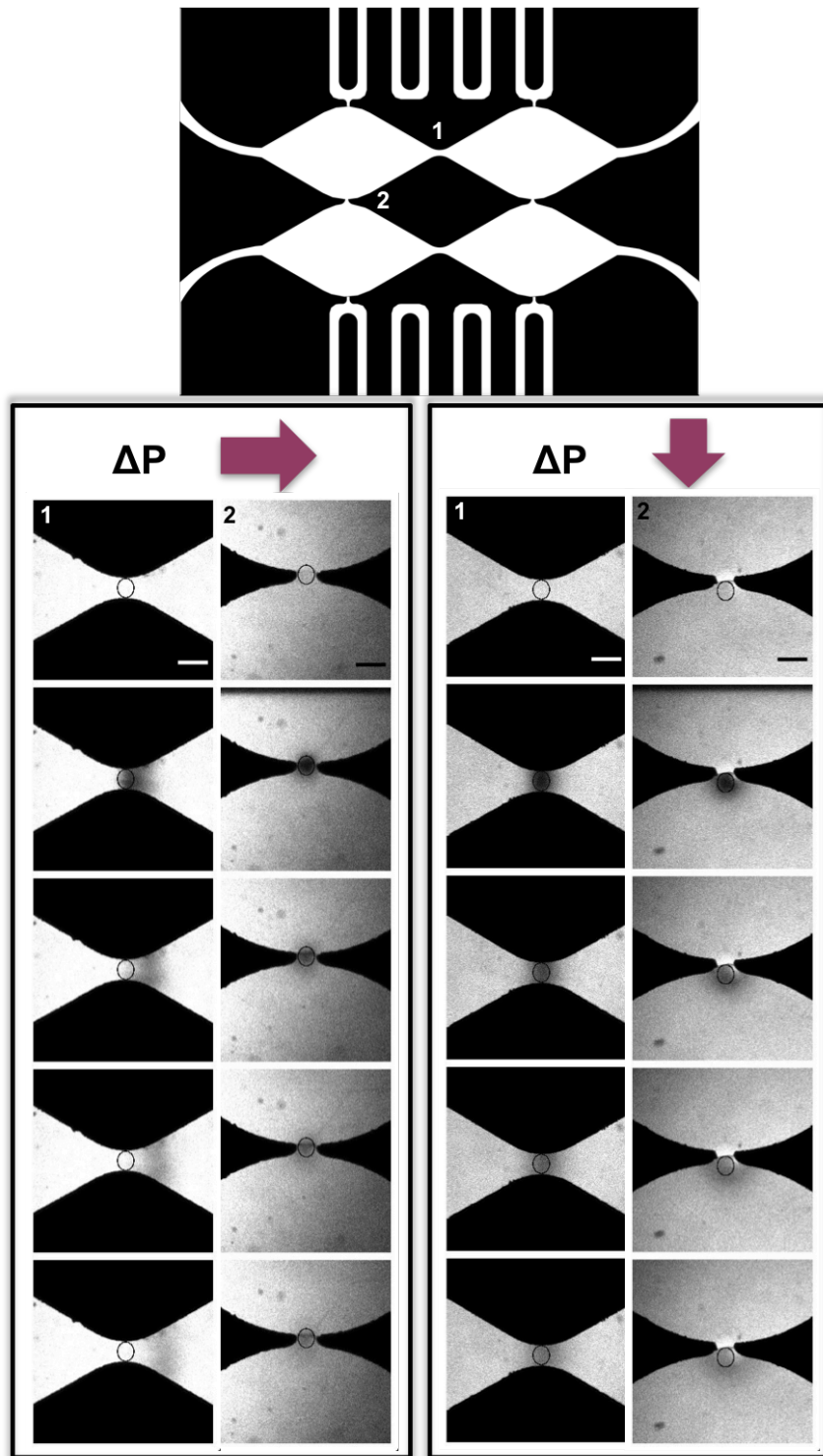


Figure 3.3. Fluorescence recovery after photobleaching (FRAP) validation of simulated interstitial flow velocity results.

3.4.3 Interstitial flow mediates cellular communication in the vasculogenesis process

To show the versatility of our platform for potential multicellular culture studies, we sought to investigate the effect of interstitial flow on the process of vasculogenesis. It is well known that interstitial flow can stimulate vasculogenesis and influence vessel formation through the redistribution of cell-secreted morphogens (92). To this end, we tested four different cellular patterning conditions (Table 3.1), to investigate the role of stromal cell-derived cytokines in the morphogenesis of endothelial-derived capillary networks.

Figure 3.4 presents the qualitative and quantitative features of the *in vitro* vessel networks formed within the microfluidic device under the two interstitial flow configurations. Cells remained viable under flow conditions through 1 week of culturing. Vacuoles consistent with early lumen formation were noted as early as two days in all conditions (data not shown). In devices where the top tissue compartment contained both ECFCs and NHLFs (condition 1; Figure 3.4A,B), a robust and interconnected network of vessels formed in a similar fashion for both interstitial flow conditions tested (i.e., longitudinal and transverse flow). In devices where ECFCs were seeded alone, non-continuous vascular structures were observed when exposed to the longitudinal flow condition (Condition 2-4; Figure 3.4D,F,H). However, as the interstitial flow condition was adjusted to allow for the ECFCs exposure to soluble factors originating from the NHLFs or conditioned media (i.e., transverse flow), an interconnected network was restored (Condition 3-4; Figure 3.4C,E,G). Quantitatively, an interconnected network is characterized by a large total vessel length, a high branching density, and a low density of endpoints (Figure 3.4I-K).

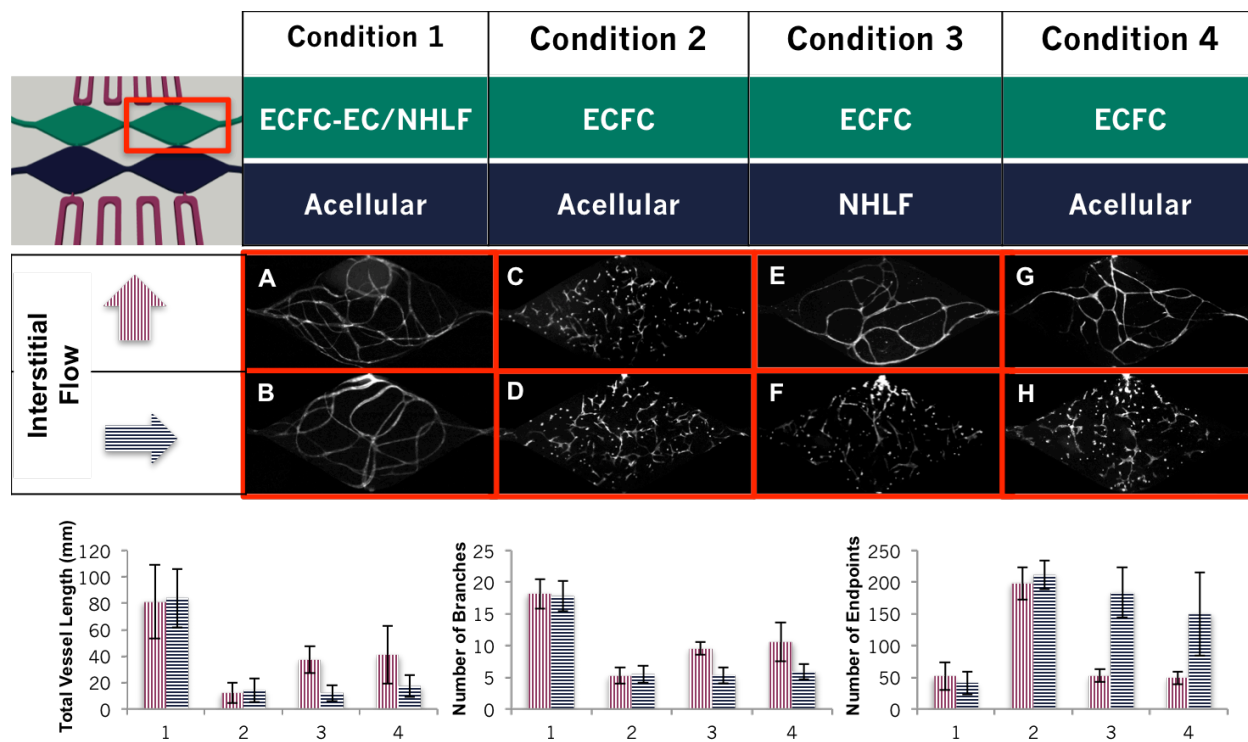


Figure 3.4. Formation of 3D *in vitro* interconnected vessel networks is depended on interstitial flow-driven communication between ECFC-ECs and NHLFs.

3.4.4 Potential applications and utility of the platform

While our studies have demonstrated the utility of our platform, we understand its potentially broad diagnostic and therapeutic applications. For instance, the platform may be used to investigate the role of microenvironmentally-derived paracrine factors in stem cell pluripotency, differentiation, and growth (106). Similarly, we can study the role of the tumor microenvironment on tumor growth and vascularization. We have conducted preliminary studies where one tissue channel simulated a vasculogenesis-like process and the parallel tissue channel simulated a tumor tissue. The pressure within these compartments was manipulated to control the direction and magnitude of interstitial fluid flow. This flexibility can encourage the development of one stromal compartment over the other, as needed.

Cells in the device remained viable through 1 week of culturing (Figure 3.5). Vessel formation was observed in the chamber containing ECFC-ECs/NHLFs in all conditions. ECFC-ECs labeled with fluorescent lipophilic dye were observed to sprout into the tumor chamber (Figure 3.5B), when interstitial flow was arranged in the transverse direction (y-axis) as early as day 4. In the presence of stromal cells, SW620s tumor cells were found to increase 60-fold in area over the duration of the experiment. Without stromal cells, tumor growth was significantly impaired.

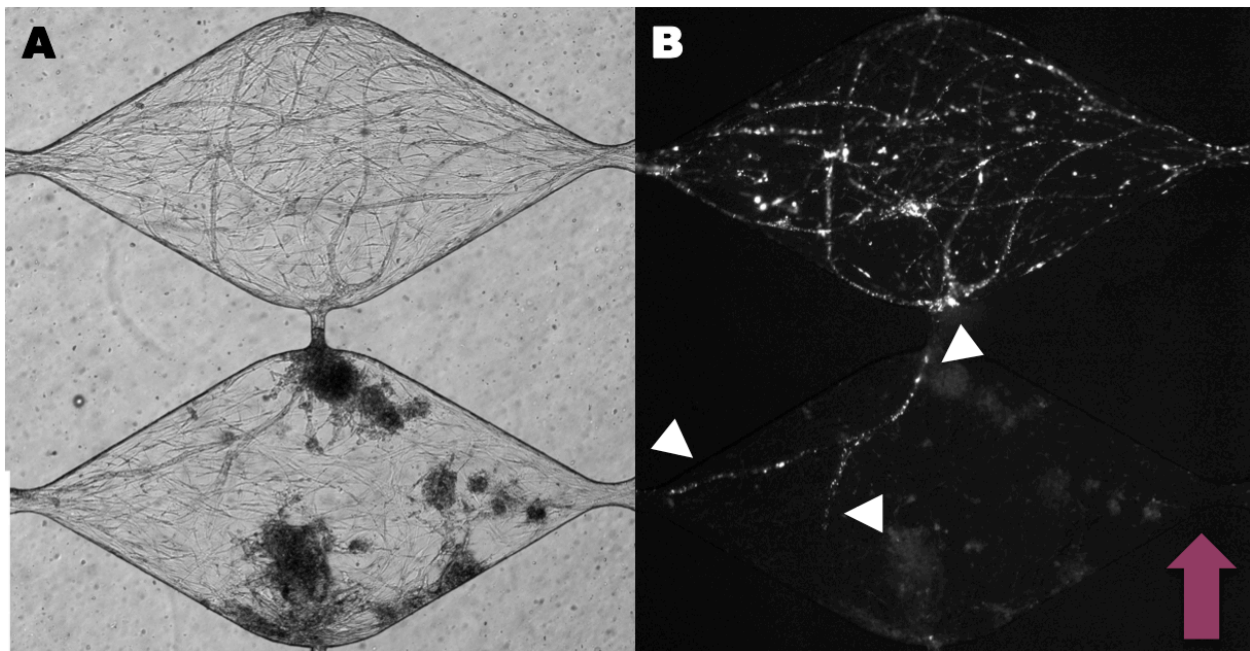


Figure 3.5. Tumor spheroid growth and microvessel network formation in four-chambered microfluidic device.

CHAPTER 4: A Microfluidic Model of Tumor Cell Intravasation and Extravasation

4.1 Introduction

Cancer mortality increases significantly following the ability of the primary tumor to metastasize (25, 107, 108). The process of cancer metastasis consists of a series of interrelated events that include primary tumor tissue invasion, intravasation (lymphatic or vascular), adhesion to the vascular wall, extravasation, and colonization of the distant site. More recently it has been noted that the tumor microenvironment can influence some of these key steps. In epithelial-derived tumors, for example, a dedifferentiation process to a migratory mesenchymal cell phenotype – also known as epithelial-mesenchymal transition (EMT) – is stimulated by factors released from macrophages (52). The precise mechanisms for much of these tumor-microenvironment interactions remain unknown, and may be patient- and tumor-specific. An improved understanding of these mechanisms has the potential to identify effective alternatives or complimentary approaches in the overall management of the disease.

Current *in vivo* and *in vitro* models provide a limited understanding of the metastatic process. A great deal of knowledge has been acquired from simple 2D cancer systems such as parallel plate flow chambers, used to study inflammation-mediated tumor cell adhesion mechanisms (109), and scratch/wound assays, used to investigate tumor cell migration and invasion mechanisms (110). Such 2D systems lack the structural architecture and tissue heterogeneity that are known to impact cancer cell biology and that can now be achieved using 3D models. A growing body of evidence also demonstrates that cells in 3D

cultures, including tumor cells, can display significant phenotype plasticity and can even respond differently to same treatment (61, 82–84). Alternatively, *in vivo* animal models can replicate the heterogeneity and complexity of the disease with high fidelity. Complex intravasation and extravasation mechanisms have been studied using models such as the chick embryo (68, 111), rat (112, 113), or zebrafish (114). However, these systems are costly, provide limited temporal resolution to study time-dependent events in the metastatic process, and may fail to reproduce important features of human tumors (84).

More recently, the field of microfluidics has provided dynamic, controllable, and compelling 3D models of human physiology that can potentially be used to augment our understanding of tumor progression and metastasis (115–117). These model systems have been coined “organ-on-a-chip”, or in the case of cancer “tumor-on-a-chip”. Despite recent advances in tumor-on-a-chip devices, there is still a need to develop models with perfused vasculature to mimic this critically important feature of metastasis and the tumor microenvironment. In the section below, we present a microfluidic-based platform of the tumor microenvironment characterized by a perfused human microvessel network, and demonstrate its potential in mechanistic studies of tumor cell extravasation and intravasation.

4.2 Materials and Methods

4.2.1 Cell culture

Human endothelial colony forming cell-derived endothelial cells (ECFC-ECs) were derived from cord blood as previously described by our lab (81). The ECFC-ECs were expanded in 1% gelatin-coated flasks in endothelial growth medium-2 (EGM-2; Lonza,

Wakersfield, MD), and were used at passages 4-6 during the experiments. Commercially available normal lung human fibroblasts (NHLFs; Lonza) were grown in fibroblast growth media (FGM; Lonza) and used at passages 5-7. Human colon adenocarcinoma cells (SW620s) were purchased from ATCC and grown in DMEM containing 10% FBS, 2mM glutamine, and 100 U/mL antibiotic/antimycotic (Gibco, Basel, Switzerland). All cells were cultured in a humidified incubator at 37°C, 5% CO₂, and 20% O₂ prior to introduction in the microfluidic device.

4.2.2 Lentiviral transduction of tumor cells to constitutively express fluorescence

To study the invasiveness and growth properties of SW620s, we transduced the cells with a titer of a lentiviral vector produced in HEK 293T cells. To prepare the vector, HEK293T cells were cultivated in a 6-well plate at a concentration of 5.0×10^5 cells/well in DMEM containing 10% fetal bovine serum (FBS) and depleted of sodium pyruvate (NaP). The cells were allowed to incubate for 24 hours at 37°C with humidified air containing 5% CO₂. Following the incubation period, a solution containing 250 µL of Opti-MEM (Invitrogen) and 6 µg of plasmid DNA (1.5 µg pRRLSIN.cPPT.PGK-GFP.WPRE, 0.75 µg pMDLg/pPRE, 0.3 µg pRSV-Rev, and 0.45 µg pMD2.G; Addgene, Cambridge, MA) was incubated at room temperature for 25 minutes. Separately, a solution of 7.5 µL of Lipofectamine 2000 (Invitrogen) and 250 µL of Opti-MEM was incubated at room temperature for 5 minutes. Both solutions were mixed well and added drop-wise to each well containing HEK293T cells. After 24 hours, the content of each well was replaced with fresh DMEM. After 48 hours, the supernatant containing the virus was collected, purified via centrifugation, and stored at -80°C for further use.

A T-75 flask containing roughly 50% confluent SW620s was incubated overnight with the mixture of 2 mL of the viral titer, 6 μ L of 10 mg/mL polybrene (Milipore, Billerica, MA), and 8 mL of DMEM. The resulting transduction efficiency was measured to be greater than 90%.

4.2.3 Microfluidic device fabrication

Standard soft lithography and replica molding processes were utilized to fabricate the microfluidic device. A master mold was created via the ultraviolet patterning of a 100 μ m thick photoresist, SU-8 (MicroChem, Newton, MA) on a silicon wafer. A polydimethylsiloxane (PDMS; Dow Corning, Elizabethtown, KY) mixture composed of 10:1 (w/w) base to curing agent was poured over the master mold and thermally cured at 65°C overnight. Once fully cured, the PDMS was cut and peeled off the mold, leaving a negative imprint of the 4-chambered design pattern. Inlet and outlet holes were punched into the PDMS piece to allow for extracellular matrix and cell culture media injection. All debris was removed from the PDMS piece, followed by an oxygen plasma treatment for 3.5 mins at 250 mTorr. A 500-750 μ m thick PDMS sheet and a 130-170 μ m thick glass coverslip (Thermo Fisher Scientific, Waltham, MA) were simultaneously plasma treated and covalently bonded to the PDMS piece to seal the channels of the device and provide mechanical support, respectively. The completed device was then baked at 120°C for a few minutes to invert the hydrophilic properties acquired during the plasma treatment process. Large glass reservoirs were then attached to the inlet and outlet holes of the fluidic lines, on top of the PDMS slab, and were cured overnight at 65°C. To sterilize and prepare the device for cell culturing, the device was autoclaved at 120°C prior to the experiment.

4.2.4 Cell loading in microfluidic device

For tissue preparation, cells were trypsinized and resuspended in 10 mg/ml bovine fibrinogen (Sigma-Aldrich, St. Louis, MO) dissolved in 1x Dulbecco's Phosphate Buffered Saline (DPBS; Gibco). Cells were mixed with the fibrinogen solution to a final concentration of 2.5×10^6 ECFC-ECs/mL, and 5.0×10^6 NHLFs/mL. Thrombin (Sigma-Aldrich) was added to the cell-fibrinogen mixture to yield a final concentration of 3 U/mL to begin the gel polymerization process, and was pipetted quickly into the tissue compartments. The device was then incubated at 37°C for 1 hr to finalize the fibrin polymerization. The microfluidic channels were then coated with 25 ug/mL human fibronectin (Sigma-Aldrich) for 1h. Subsequently, a concentrated solution of ECFC-ECs (6×10^6 cell/mL) in EGM-2 medium was introduced into the entire lengths of both adjacent fluidic channels. The ECFC-ECs were allowed to attach under static conditions in a 20% O₂ incubator for 12 hours, after which a fully supplemented cell culture medium was introduced into the channels and a set of microfluidic jumpers were installed to complete the connection. The volume of each inlet and outlet vial was adjusted in order to create a dynamic culturing environment that consisted of a pressure gradient across the tissue. The microfluidic platform was next placed in a 5% O₂ incubator for the remainder of the experiments (7-21 days). Media volumes were replaced and readjusted every 24-48 hrs to maintain the desired pressure drop across the tissue channel for the duration of the experiment.

4.2.5 Analysis of endothelial cell adhesion to PDMS surfaces

Bright field images of ECFC-ECs were captured using an inverted microscope (Olympus IX83) 12 hours post-insertion and incubation of the ECFC-ECs in the microfluidic

channels. Using ImageJ software (National Institutes of Health), the outline of each cell was manually traced and the total coverage area was calculated. Cells from 3 different experiments (3 fields of a total 432.8 mm² PDMS surface area in each experiment) were used, and the percentage coverage was averaged for each fibronectin coating condition tested.

4.2.6 Quantification of vessel network formation

After 7-21 days in the incubator, the microtissues within the microfluidic device were subjected to immunofluorescent staining with CD31-antibodies using a modified staining protocol (71, 81). The microtissues were initially fixed in 10% formalin that was introduced through the adjacent fluidic channels for 18 hrs. The staining process consisted of exposing the microtissues to mouse anti-human CD31 antibody (Dako, Carpinteria, CA) for 1-2 days, followed by Alexa-Flour 488-conjugated goat anti-mouse IgG (Invitrogen, Grand Island, NY) for an additional 1-2 days. Images of the stained microvessels were taken using an inverted fluorescence microscope (Olympus IX83, Central Valley, PA). Vessels stained positive for CD31 were analyzed using AngioTool (102), a software for quantitative assessment of various vessel parameters. We acquired images confirming lumen formation and intravascular cell migration were acquired using laser scanning confocal microscopy (Zeiss LSM 510 Meta)

4.2.7 Assessment of tumor growth

The devices were imaged once a day and their GFP signals were captured using an inverted fluorescent microscope (Olympus IX83). The area of the GFP signal was measured

using an in-house Matlab script and expressed as a percentage of the total tissue chamber area to determine the growth rate.

4.2.8 Perfusion analyses and extravasation experiments

Flow in formed capillaries was assessed in the first week of culturing by adding 1 μ m polystyrene fluorescence microbeads (Invitrogen) into the arteriole microfluidic channel, and were observed as they entered the capillaries via the anastomotic connections. Images were captured at 10 Hz using an Olympus IX83 inverted microscope and a B/W CCD digital camera (Hamamatsu ORCA). Microspheres were manually tracked in perfused tissues from three separate microfluidic chips using ImageJ. We also used fluorescent dextran (70 kDa; Sigma-Aldrich) as an alternate method to assess vessel perfusion, which was introduced into the arteriole microfluidic channel and visualized in the fluidic lines and central chambers using fluorescent microscopy.

Following the confirmation of vessel perfusion, tumor cells at a concentration of 1×10^6 cell/mL were introduced into the arteriole microfluidic channel and were observed to flow into the capillary networks. Monitoring of tumor growth was conducted over the following two weeks.

4.2.9 Statistical analysis

Statistical analyses were performed using one-way analysis of variance (ANOVA) with StatPlus (AnalystSoft Software). Comparisons between groups were made with the Student's t-test for multiple comparisons. All data are presented as the mean \pm standard deviation. Results are considered to be statistically significant for $p < 0.05$.

4.3 Results

4.3.1 Device construction for optimal vessel perfusion

The construction of this modified microfluidic device (Figure 4.1) was informed by our previous observations of perfused vessel network formation occurring *in vitro* when exposed to supraphysiological interstitial flow (71). The device consisted of a series of three mm-sized, diamond-shaped tissue chambers that house the cells within a 3D fibrin hydrogel. On both sides of the tissue chambers are two fluid-filled microfluidic channels connected via micropores ($30\ \mu\text{m} \times 100\ \mu\text{m}$), which provide the developing tissue chamber with the chemical and mechanical stimuli conducive to microvessel perfusion. Similar to our previously published platforms (71, 73, 74), the convective delivery of media is achieved through hydrostatic pressure differences. The microfluidic channels are interrupted at specific positions (colored squares; Figure 4.1), and connected with removable Tygon™ tubing. This configuration allows for direct access to the tissue chamber when necessary (e.g., immunofluorescent antibody labeling, confirmation of perfused vasculature, introduction of circulating cells) without jeopardizing the control of critical convective flow during the tissue development stages.

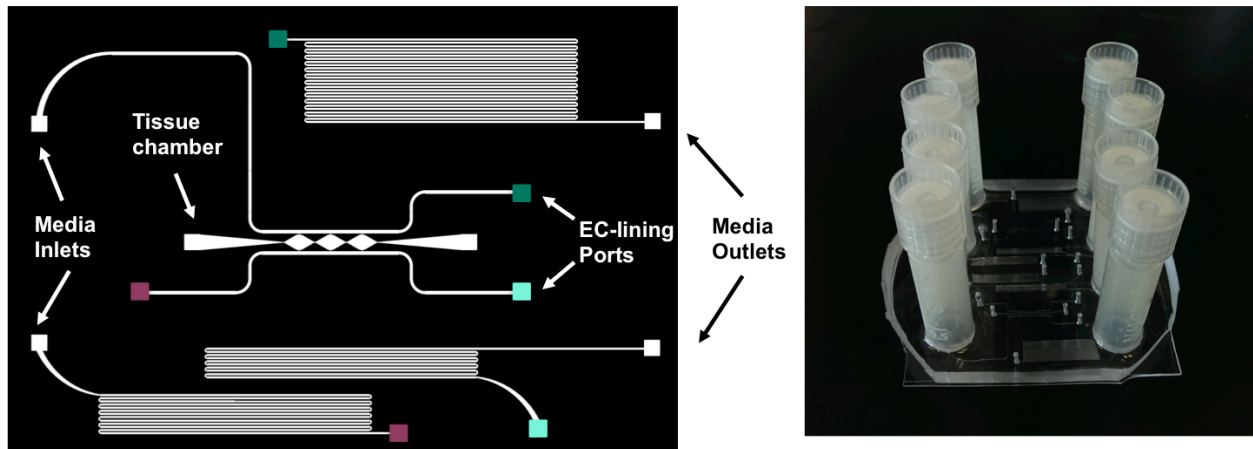


Figure 4.1 Microfluidic device used to simulate tumor microenvironments. (A) Schematic illustrating the use. (B) Macroscopic picture of the microfluidic device platform and media reservoirs.

4.3.2 ECFC-EC attachment to PDMS is dependent on non-competitive FN absorption

An additional feature of the device is its ability to seed ECFC-ECs in specific sections adjacent to the tissue chamber (Figure 4.1). Given the time frame of the experiments (i.e. up to 21 days in culture), we sought to investigate the attachment efficiencies of ECFC-ECs at different time points and their effect on the resulting perfusion of the vascular network within the tissue chamber. ECFC-ECs seeded on day 0 in FN-coated PDMS microchannels showed an 85% increased attachment compared to untreated microchannels (Figure 4.2a, b). In comparison to the untreated PDMS surface, the ECFC-ECs' attachment efficiency on day 7 in the newly FN-coated PDMS microchannels increased by 60%, but this efficiency was 25% less than the day 0 ECFC-EC seeding condition (Figure 4.2c). These differences could be dependent on the time at which the channels were exposed to FN coating. When the PDMS microchannels were coated with FN on day 0, followed by a week-long exposure to EGM-2 culture media, the ECFC-EC attachment on day 7 showed an increase of 20% compared to samples where FN-coating occurred on the same day as seeding (Figure 4.2d).

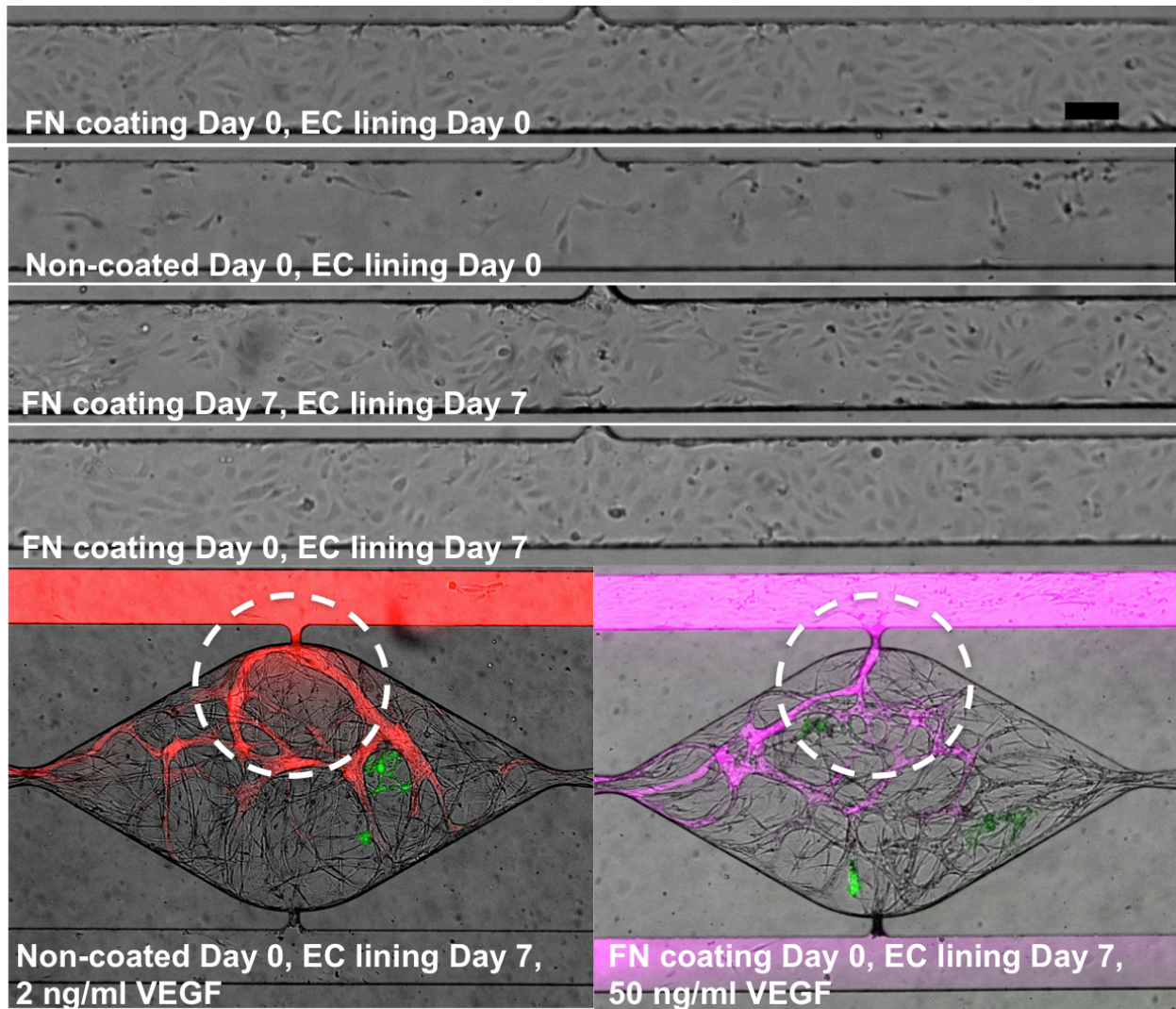


Figure 4.2 ECFC-EC attachment on microfluidic on microfluidic channel mimic functional arteriole and venule compartments.

The sprouting of ECFC-ECs from the microfluidic channel into the tissue chamber was dependent on the quantity of attached cells and the concentration of VEGF present in the media, rather than on the time at which the ECFC-ECs were introduced into the microchannels. Confirming previously reported data (76, 117), 50 ng/ml VEGF stimulation supported angiogenesis sprouting into the tissue chamber, compared to the quiescent effect of 2 ng/ml VEGF supplemented EGM-2 media. The induction of ECFC-EC sprouting is

a critical process to ensure proper and accelerated anastomosis, through the connecting micropores, with the self-assembled capillary bed within the tissue chamber. A proper link between these two compartments can ensure that the fluid flow occurs exclusively through the perfused network instead of leaking into the interstitial space at their interface (Figure 4.2e. f).

4.3.3 Platform to study intravascular tumor cell adhesion and “extravasation”

In order to investigate the process of extravasation, a vascular network from an ECFC-EC/NHLF co-culture within a 3D fibrin gel was grown in the tissue chamber for a period of 6-9 days. The microfluidic channels were lined with ECFC-ECs at day 0. During this timeframe, the vascular network anastomosed with the ECFC-EC sprouts originating from the adjacent microfluidic channels. Perfusion through the capillary network can be achieved within a week of culturing, much faster than we previously reported (71).

Following the confirmation of intravascular perfusion in the vascular network, EGFP-labeled SW620s were introduced into ECFC-EC lined microfluidic channels via the EC-lining ports. These ports are easily accessible through the removal of the Tygon™ tubing, which can be reattached after the insertion of the tumor cells. Through the decoupling of the two adjacent microchannels a pressure gradient can be achieved across the tissue channel. SW620s entering the EC-lined microfluidic channels were observed to flow through the micropores and into the capillary network, achieving physiological fluid velocities that ranged between 625 and 240 $\mu\text{m/s}$ (video; <http://youtu.be/47oh3qXqyIM>). The rate SW620 attachment to the EC-wall was 5% in areas where average fluid velocities descended to values below 110 $\mu\text{m/s}$.

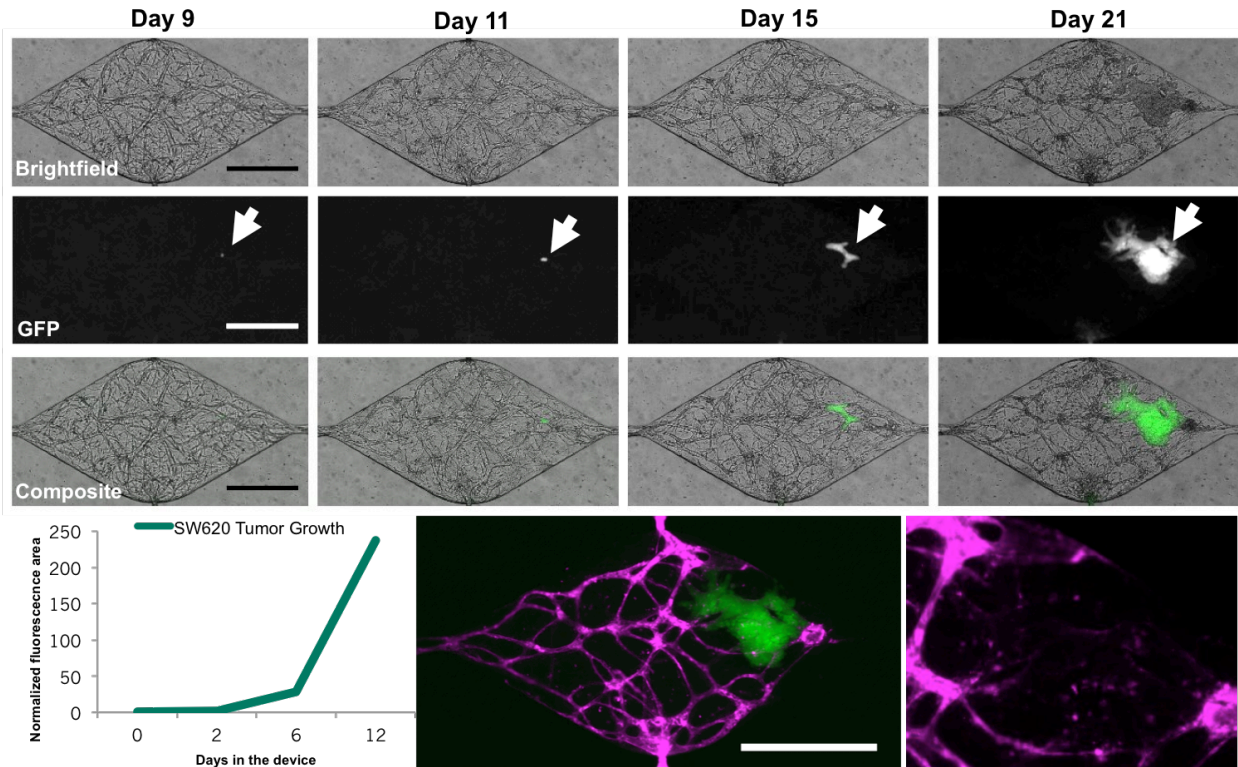


Figure 4.3. Microfluidic platform may be used to mimic extravasation events.

Reconnecting the device tubing to its original configuration restored the culture conditions, prior to insertion of the SW620 cells. The proliferation and migration of the tumor cells were monitored throughout the remainder of the experiment (Figure 4.3a, b, c). A simple growth curve based on the total area of fluorescence in a 2D image of the device (Figure 4.3d) shows that the SW620s area increased 250 fold within 15 days. Interestingly, SW620 growth initially (first 4-6 days) appeared to be confined to the boundaries of the microvasculature wall and to conform to the shape of the microvasculature. Eventually, the tumor growth compromised the integrity of the vessel wall, thus allowing the tumor to grow unconstrained into the fibrin ECM. CD31 labeling of the ECFC-ECs on day 21 shows positively stained fragments of the ruptured wall around the periphery of the tumor mass (Figure 4.3e, f). In addition, the presence of the tumor had a detrimental effect on the

overall vessel network. On day 21, the resulting average area of the vessel network was $29.3 \pm 1.7 \%$ and the average connectedness index of the network was calculated at 1.15 ± 0.07 compared to previous reports (71).

4.3.4 Platform to study tumor angiogenesis and intravasation

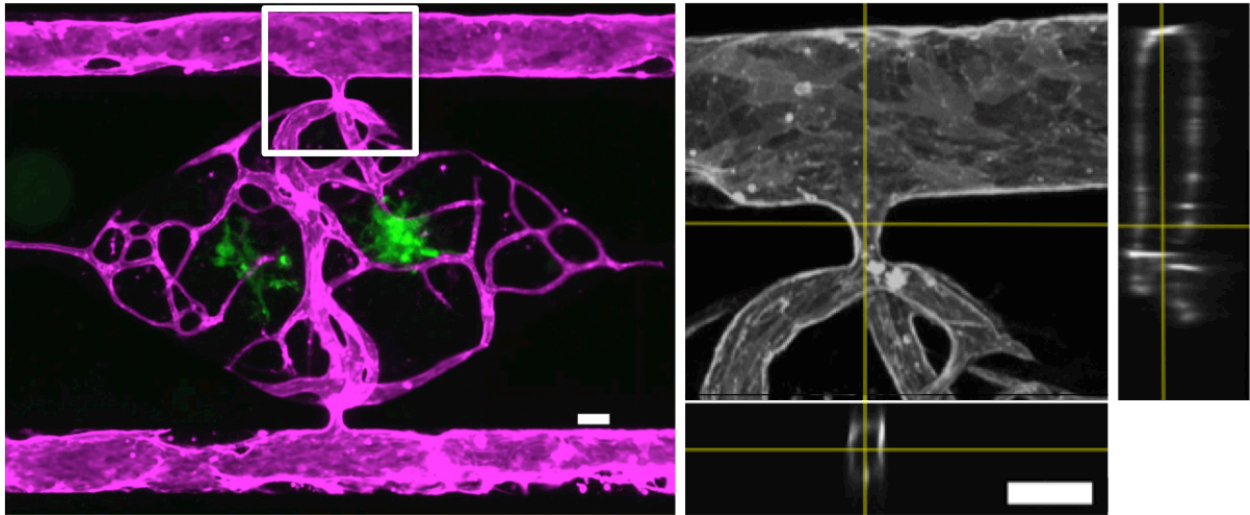


Figure 4.4. Confocal imaging of the microtissue confirms anastomosis.

Alternatively, we can use the platform to investigate early events in tumor intravasation. An ECFC-EC/NHLF/SW620 tri-culture was introduced into the tissue chamber as a single-cell suspension within a fibrin matrix, and was grown for a period of 21 days. For the duration of the experiment, we continuously tracked vessel network formation and tumor growth. During the first week, the vascular network forms and is morphologically indistinguishable from those with no tumor cells (71). Namely, the vessel percentage area was measured to be $32 \pm 6\%$, and the vessel connectedness index was 0.15 ± 0.05 . Similarly, confocal imaging of the vessels in the tumor microenvironment, which were stained for CD31 on day 7, demonstrated the functional anastomosis of the developed vasculature with the ECFC-EC sprouts originating from the adjacent microfluidic channel (Figure 4.4, video: <http://youtu.be/GMpesksNPmM>).

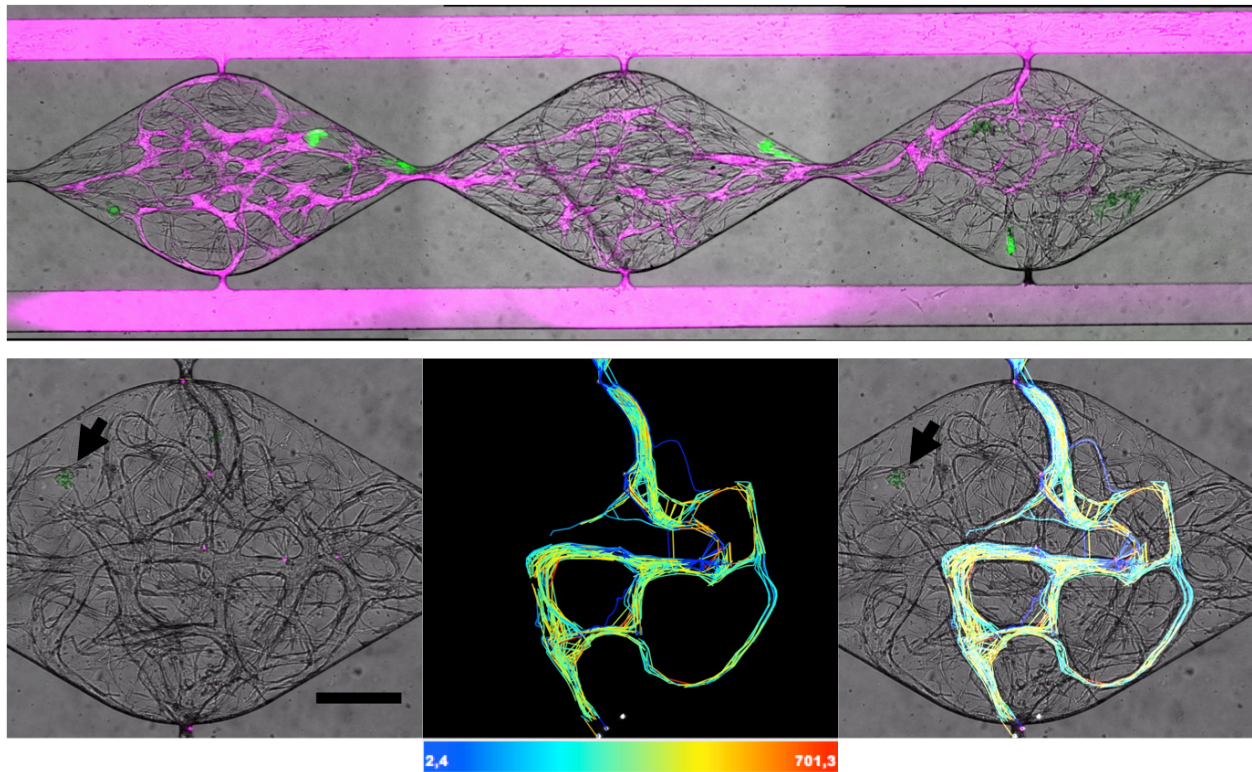


Figure 4.5. Assessment of vascular perfusion in the vessel network within the tumor microenvironment.

Intraluminal vessel perfusion was assessed following the confirmation of anastomosis, on days 7-10. Various size fluorescent dextran (70 kDa and 150 kDa) were introduced in the microfluidic channel and allowed to enter the formed vascular bed through a pressure gradient across the tissue (Figure 4.5a). Dextran was retained by the vascular wall and perfusion showed approximately $75\pm 5\%$ functional vessels of different diameters ranging from $12\text{-}33\ \mu\text{m}$. Insertion of $1\ \mu\text{m}$ beads demonstrated a different facet of the developed network. Despite the high yield of perfusion observed via fluorescent dextran, beads followed trajectories that only encompassed $45\pm 3\%$ of the developed vessel network. Particle tracking showed that near physiological fluid flow velocities of 761 to $250\ \mu\text{m/s}$ could be achieved within the tumor microenvironment (Figure 4.5b)

Tumor growth was simultaneously monitored during the tissue culturing process. SW620 viability was maintained under interstitial flow conditions for a period of 21 days (Figure 4.6a). SW620s were initially introduced as a single cell suspension in conjunction with the ECFC-EC/NHLF co-culture, and over time they developed into tumor masses resulting from self-proliferation and aggregation with other nearby masses. Over this time span, the tumor growth area increased 35 fold.

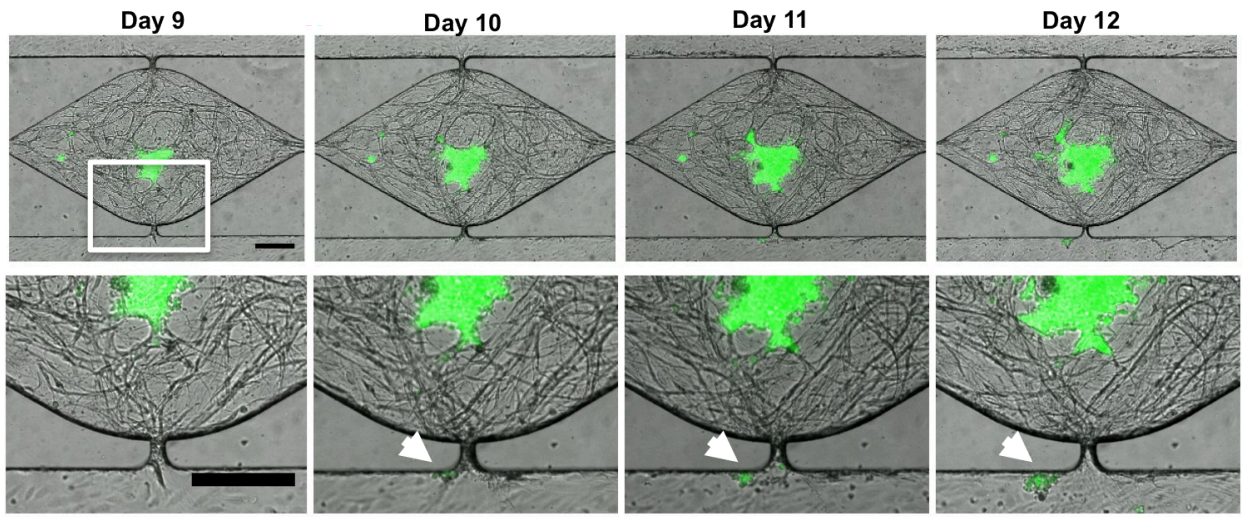


Figure 4.6. Microfluidic platform may be used to mimic intravasation events.

4.4 Discussion

Over the past decade, the goal of recapitulating the tumor microenvironment *in vitro* has benefited greatly from the significant advances in soft lithography and other microfabrication techniques (118). These new systems are aimed at addressing the shortcomings of 2D *in vitro* assays and the complexity of *in vivo* animal models (84, 119, 120). To add to this growing body of literature, we have developed a novel microfluidic system of the tumor microenvironment to study relevant mechanisms in the metastatic cascade. The microfluidic platform is adaptable and allows us to investigate two important process of tumor metastasis: intravasation and extravasation. Our system features human

derived perfused capillaries and allows for real-time visualization of the interaction between endothelial cells, the stroma and tumor cells in 3D. The device provides flexibility and reproducibility in a controlled environment, and is potentially adaptable for high-throughput screening that may be useful for the discovery of anti-tumor drugs.

Our approach to create a perfused vascular bed uses a combination of synthetic and naturally forming vessels, exploiting the advantages of each. The self-assembly of vessel networks in the central tissue compartment allow us to replicate an *in vivo* like process of vasculogenesis, which responds to relevant environmental cues such as stromal cell stimulation and interstitial flow. Adjacent synthetic vessels allow us to mimic a functional arteriole and venule, which form sprouts into the tissue chamber and encourage anastomosis with the developing microvasculature. Once the connection between the EC-lined channel and the self-assembled EC/fibroblast network occurs, we are able to control and directly access the resulting perfused vasculature for various biological inquiries. To achieve this feature, we exploited the property of PDMS to non-specifically adsorb proteins and small molecules due to its hydrophobicity and porosity (121–124). Though previous groups had developed techniques to attach endothelial cells into a FN treated PDMS surface (76, 117), our focus was on gaining temporal control of anastomotic process.

Two leading hypothesis have been proposed to explain the process of tumor cell adhesion at the distant site are the “seed and soil” hypothesis and the “mechanical trapping” hypothesis (125–128). Due to the difficulty of observing key steps of the metastatic process *in vivo* and the inability of current *in vitro* systems to properly recreate these events, several contradictory results regarding these theories have been reported.

Our platform yields a capillary bed with heterogeneous vessel diameters, flow rates, and shear stresses; which can be imaged in real-time to highlight the critical steps of the interactions between the endothelium and circulating tumor cells. To illustrate this capability we used colon adenocarcinoma cells, SW620, which were shown to adhere to the endothelial cell wall in areas where the flow and shear stress were low, rather than in vessels with restricting diameters. In fact, real-time tracking of the circulating tumor cells during the initial seeding stages showed that the tumor cells do not flow through small diameter vessels, even though these vessels are perfused. These observations suggest that intraluminal shear stresses may play a significant role in the tumor cell – endothelial cell adhesion process at the distant site.

To study the interaction of adhered tumor cells with the endothelium, our device allows for continuous vascular perfusion where the tumor cells residing in the intravascular space are exposed to physiological shear stresses. Interestingly, using the SW620 tumor cells, we observe that these cells do not employ a classical method of extravasation where they migrate across the endothelium. Instead, the SW620s remain attached within the intravascular space of the vessel network. This behavior is consistent with previous observations of *in vivo* intravascular adhesion in mouse lungs (112), as well as previously reported invasiveness indexes (129). Other groups have reported on similar microfluidic platforms where tumor cells transmigrate across the endothelial cell barrier; however, alternate tumor models of higher invasiveness potential were employed in these studies (116, 130). This highlights the heterogeneity in tumor cell behavior between different cells lines. Our platform is flexible enough to allow for a thorough screening of a plethora of tumor cell lines of varying degrees of invasiveness.

Previous models of vasculogenesis and angiogenesis have shown the capability to study specific vascular related processes, but this is the first time a perfused network is shown in an *in vitro* model of the tumor microenvironment. Here we developed a system where the network is entirely composed of endothelial progenitor cells and a vasculogenesis process – aided by stromal cells – is sufficient to form a network. Our results suggest that tumors may develop in such an environment with minimal impact on the developing vasculature within the early stages. Once the tumor exceeds a critical stage – after 1 week of culture – and perfusion is established within the self-assembled network, the tumor grows uncontrollably, invading the capillary network and in turn causes an unstable vasculature to form.

In summary, we have demonstrated the recapitulation of the tumor microenvironment in an *in vitro* microfluidic system. Our results validate a platform where you can investigate intravasation and extravasation events of metastasis. Some of the highlights of our system include the formation of perfused vascular networks, which provide vital interactions with the tumor cells. In addition, the platform is amenable to real-time imaging; allowing for the visualization of relevant time-dependent steps in the metastatic process. This system has the potential to be used as for broad diagnostic and therapeutic applications.

REFERENCES

1. W. L. Donegan, in *Breast Cancer*, N. L. Winchester DJ, Winchester DP, Hudis CA, Ed. (B.C. Decker, Ontario, 2006), pp. 1–14.
2. Cancer. *World Heal. Organ.* (2014), (available at <http://www.who.int/mediacentre/factsheets/fs297/en/>).
3. QuickStats: Age-Adjusted Death Rates for Heart Disease and Cancer --- United States, 1999--2009*. *Centers Dis. Control Prev.* (2011), (available at http://www.cdc.gov/mmwr/preview/mmwrhtml/mm6021a6.htm?s_cid=mm6021a6_e&source=govdelivery).
4. G. Kolata, Playing it Safe in Cancer Research. *New York Times* (2009), (available at <http://www.nytimes.com/2009/06/28/health/research/28cancer.html?pagewanted=1>).
5. D. Hanahan, R. A. Weinberg, The hallmarks of cancer. *Cell.* **100**, 57–70 (2000).
6. D. Hanahan, R. A. Weinberg, Hallmarks of cancer: the next generation. *Cell.* **144**, 646–74 (2011).
7. S. L. Floor, J. E. Dumont, C. Maenhaut, E. Raspe, Hallmarks of cancer: of all cancer cells, all the time? *Trends Mol. Med.* **18**, 509–15 (2012).
8. Y. Lazebnik, What are the hallmarks of cancer? *Nat. Rev. Cancer.* **10**, 232–3 (2010).
9. C. Sonnenschein, A. M. Soto, The aging of the 2000 and 2011 Hallmarks of Cancer reviews: A critique. *J. Biosci.* **38**, 651–663 (2013).
10. P. Fedi, A. Kimmelman, S. A. Aaronson, *Growth Factor Signal Transduction in Cancer* (2000).
11. D. J. Slamon *et al.*, Human breast cancer: correlation of relapse and survival with amplification of the HER-2/neu oncogene. *Science.* **235**, 177–182 (1987).
12. D. Harari, Y. Yarden, Molecular mechanisms underlying ErbB2/HER2 action in breast cancer. *Oncogene.* **19**, 6102–6114 (2000).
13. P. P. Di Fiore *et al.*, erbB-2 is a potent oncogene when overexpressed in NIH/3T3 cells. *Science.* **237**, 178–182 (1987).
14. M. E. Lukashev, Z. Werb, ECM signalling: Orchestrating cell behaviour and misbehaviour. *Trends Cell Biol.* **8** (1998), pp. 437–441.

15. F. G. Giancotti, Integrin Signaling. *Science (80-.)*. **285** (1999), pp. 1028–1033.
16. A. E. Aplin, A. Howe, S. K. Alahari, R. L. Juliano, Signal transduction and signal modulation by cell adhesion receptors: the role of integrins, cadherins, immunoglobulin-cell adhesion molecules, and selectins. *Pharmacol. Rev.* **50**, 197–263 (1998).
17. R. H. Medema, J. L. Bos, The role of P21-Ras in Receptor Tyrosine Kinase Signaling. *Crit. Rev. Oncog.* **4**, 615–661 (1993).
18. T. Hunter, Oncoprotein networks. *Cell.* **88**, 333–46 (1997).
19. K. W. Kinzler, B. Vogelstein, Lessons from hereditary colorectal cancer. *Cell.* **87** (1996), pp. 159–170.
20. C. Rommel, E. Hafen, Ras - A versatile cellular switch. *Curr. Opin. Genet. Dev.* **8** (1998), pp. 412–418.
21. J. Downward, Mechanisms and consequences of activation of protein kinase B/Akt. *Curr Opin Cell Biol.* **10**, 262–267 (1998).
22. T. D. Tlsty, L. M. Coussens, Tumor stroma and regulation of cancer development. *Annu. Rev. Pathol.* **1**, 119–50 (2006).
23. J. A. Joyce, J. W. Pollard, Microenvironmental regulation of metastasis. *Nat. Rev. Cancer.* **9**, 239–52 (2009).
24. M. J. Bissell, D. Radisky, Putting tumours in context. *Nat. Rev. Cancer.* **1**, 46–54 (2001).
25. G. P. Gupta, J. Massagué, Cancer metastasis: building a framework. *Cell.* **127**, 679–95 (2006).
26. M. Allinen *et al.*, Molecular characterization of the tumor microenvironment in breast cancer. *Cancer Cell.* **6**, 17–32 (2004).
27. T. D. Tlsty, Stromal cells can contribute oncogenic signals. *Semin. Cancer Biol.* **11**, 97–104 (2001).
28. M. M. Mueller, N. E. Fusenig, Friends or foes - bipolar effects of the tumour stroma in cancer. *Nat. Rev. Cancer.* **4**, 839–849 (2004).
29. M. R. Junttila, F. J. de Sauvage, Influence of tumour micro-environment heterogeneity on therapeutic response. *Nature.* **501**, 346–54 (2013).
30. A. Marusyk, K. Polyak, Tumor heterogeneity: Causes and consequences. *Biochim. Biophys. Acta - Rev. Cancer.* **1805** (2010), pp. 105–117.

31. R. Straussman *et al.*, Tumour micro-environment elicits innate resistance to RAF inhibitors through HGF secretion. *Nature*. **487** (2012), pp. 500–504.
32. D. L. Longo, Tumor Heterogeneity and Personalized Medicine. *N. Engl. J. Med.* **366** (2012), pp. 956–957.
33. T. Wilson, John H., Hunt, *Molecular Biology of the Cell, A Problems Approach* (Garland Science, New York, 4th Ed., 2002).
34. G.-O. Ahn, J. M. Brown, Role of endothelial progenitors and other bone marrow-derived cells in the development of the tumor vasculature. *Angiogenesis*. **12**, 159–164 (2009).
35. B. Bussolati, C. Grange, G. Camussi, Tumor exploits alternative strategies to achieve vascularization. *FASEB J.* **25**, 2874–2882 (2011).
36. O. M. Tepper *et al.*, Adult vasculogenesis occurs through in situ recruitment, proliferation, and tubulization of circulating bone marrow-derived cells. *Blood*. **105**, 1068–1077 (2005).
37. J. Folkman, Angiogenesis: an organizing principle for drug discovery? *Nat. Rev. Drug Discov.* **6**, 273–86 (2007).
38. P. Carmeliet, Mechanisms of angiogenesis and arteriogenesis. *Nat. Med.* **6**, 389–395 (2000).
39. J. Folkman, Tumor angiogenesis: therapeutic implications. *N. Engl. J. Med.* **285**, 1182–1186 (1971).
40. D. Hanahan, J. Folkman, Patterns and emerging mechanisms of the angiogenic switch during tumorigenesis. *Cell*. **86** (1996), pp. 353–364.
41. B. Bussolati, B. Assenzio, M. C. Deregibus, G. Camussi, The proangiogenic phenotype of human tumor-derived endothelial cells depends on thrombospondin-1 downregulation via phosphatidylinositol 3-kinase/Akt pathway. *J. Mol. Med. (Berl)*. **84**, 852–63 (2006).
42. D. Mangieri *et al.*, Angiogenic activity of multiple myeloma endothelial cells in vivo in the chick embryo chorioallantoic membrane assay is associated to a down-regulation in the expression of endogenous endostatin. *J. Cell. Mol. Med.* **12**, 1023–1028 (2008).
43. S. K. Hobbs *et al.*, Regulation of transport pathways in tumor vessels: role of tumor type and microenvironment. *Proc. Natl. Acad. Sci. U. S. A.* **95**, 4607–4612 (1998).
44. J. A. Nagy, A. M. Dvorak, H. F. Dvorak, VEGF-A and the induction of pathological angiogenesis. *Annu. Rev. Pathol.* **2**, 251–275 (2007).

45. J. W. Baish *et al.*, Scaling rules for diffusive drug delivery in tumor and normal tissues. *Proc. Natl. Acad. Sci. U. S. A.* **108**, 1799–1803 (2011).
46. P. Carmeliet, R. K. Jain, Molecular mechanisms and clinical applications of angiogenesis. *Nature.* **473**, 298–307 (2011).
47. Y. Gazit, D. Berk, M. Leunig, L. Baxter, R. Jain, Scale-Invariant Behavior and Vascular Network Formation in Normal and Tumor Tissue. *Phys. Rev. Lett.* **75** (1995), pp. 2428–2431.
48. F. Yuan *et al.*, Microvascular permeability and interstitial penetration of sterically stabilized (stealth) liposomes in a human tumor xenograft. *Cancer Res.* **54**, 3352–3356 (1994).
49. J. A. Nagy, S.-H. Chang, A. M. Dvorak, H. F. Dvorak, Why are tumour blood vessels abnormal and why is it important to know? *Br. J. Cancer.* **100**, 865–869 (2009).
50. H. Hashizume *et al.*, Openings between defective endothelial cells explain tumor vessel leakiness. *Am. J. Pathol.* **156**, 1363–1380 (2000).
51. J. Hagendoorn *et al.*, Onset of abnormal blood and lymphatic vessel function and interstitial hypertension in early stages of carcinogenesis. *Cancer Res.* **66**, 3360–4 (2006).
52. B. Z. Qian, J. W. Pollard, Macrophage Diversity Enhances Tumor Progression and Metastasis. *Cell.* **141** (2010), pp. 39–51.
53. A. P. Sappino, W. Schürch, G. Gabbiani, Differentiation repertoire of fibroblastic cells: expression of cytoskeletal proteins as marker of phenotypic modulations. *Lab. Invest.* **63**, 144–61 (1990).
54. H. Y. Chang *et al.*, Gene expression signature of fibroblast serum response predicts human cancer progression: Similarities between tumors and wounds. *PLoS Biol.* **2** (2004), doi:10.1371/journal.pbio.0020007.
55. J. A. G. Rhodin, Ultrastructure of mammalian venous capillaries, venules, and small collecting veins. *J. Ultrastruct. Res.* **25**, 452–500 (1968).
56. J. A. Rhodin, H. Fujita, Capillary growth in the mesentery of normal young rats. Intravital video and electron microscope analyses. *J. Submicrosc. Cytol. Pathol.* **21**, 1–34 (1989).
57. D. J. Crocker, T. M. Murad, J. C. Geer, Role of the pericyte in wound healing. An ultrastructural study. *Exp. Mol. Pathol.* **13**, 51–65 (1970).

58. R. A. Willis, The unusual in tumour pathology. *Can. Med. Assoc. J.* **97**, 1466–1479 (1967).
59. E. B. Brown *et al.*, In vivo measurement of gene expression, angiogenesis and physiological function in tumors using multiphoton laser scanning microscopy. *Nat. Med.* **7**, 864–868 (2001).
60. D. Fukumura *et al.*, Tumor induction of VEGF promoter activity in stromal cells. *Cell.* **94**, 715–725 (1998).
61. F. Pampaloni, E. G. Reynaud, E. H. K. Stelzer, The third dimension bridges the gap between cell culture and live tissue. *Nat. Rev. Mol. Cell Biol.* **8**, 839–845 (2007).
62. M. Cekanova, K. Rathore, Animal models and therapeutic molecular targets of cancer: utility and limitations. *Drug Des. Devel. Ther.* **8**, 1911–1922 (2014).
63. E. Svensjö, *Eur. Respir. J. Suppl.*, in press.
64. J. F. Gross, M. Intaglietta, B. W. Zweifach, Network model of pulsatile hemodynamics in the microcirculation of the rabbit omentum. *Am. J. Physiol.* **226**, 1117–23 (1974).
65. D. L. Jackson, W. P. Dole, J. McGloin, J. I. Rosenblatt, Total cerebral ischemia: application of a new model system to studies of cerebral microcirculation. *Stroke.* **12**, 66–72.
66. P. Vajkoczy, M. D. Menger, New model for the study of the microcirculation of islet grafts in hairless and nude mice. *Transplant. Proc.* **26**, 687 (1994).
67. V. Subramaniam, I. R. Vincent, M. Gilakjan, S. Jothy, Suppression of human colon cancer tumors in nude mice by siRNA CD44 gene therapy. *Exp. Mol. Pathol.* **83**, 332–340 (2007).
68. M. C. Subauste *et al.*, Evaluation of metastatic and angiogenic potentials of human colon carcinoma cells in chick embryo model systems. *Clin. Exp. Metastasis.* **26**, 1033–1047 (2009).
69. A. C. Newman, M. N. Nakatsu, W. Chou, P. D. Gershon, C. C. W. Hughes, The requirement for fibroblasts in angiogenesis: fibroblast-derived matrix proteins are essential for endothelial cell lumen formation. *Mol. Biol. Cell.* **22**, 3791–800 (2011).
70. R. Montesano, M. S. Pepper, L. Orci, Paracrine induction of angiogenesis in vitro by Swiss 3T3 fibroblasts. *J. Cell Sci.* **105** (Pt 4), 1013–1024 (1993).
71. M. L. Moya, Y.-H. Hsu, A. P. Lee, C. C. W. Hughes, S. C. George, In vitro perfused human capillary networks. *Tissue Eng. Part C. Methods.* **19**, 730–7 (2013).

72. V. Vickerman, J. Blundo, S. Chung, R. Kamm, Design, fabrication and implementation of a novel multi-parameter control microfluidic platform for three-dimensional cell culture and real-time imaging. *Lab Chip*. **8**, 1468–77 (2008).
73. Y.-H. Hsu *et al.*, Full range physiological mass transport control in 3D tissue cultures. *Lab Chip*. **13**, 81–9 (2013).
74. Y.-H. Hsu, M. L. Moya, C. C. W. Hughes, S. C. George, A. P. Lee, A microfluidic platform for generating large-scale nearly identical human microphysiological vascularized tissue arrays. *Lab Chip*. **13**, 2990–8 (2013).
75. S. Kim, H. Lee, M. Chung, N. L. Jeon, Engineering of functional, perfusable 3D microvascular networks on a chip. *Lab Chip*. **13**, 1489–500 (2013).
76. J. W. Song, D. Bazou, L. L. Munn, Anastomosis of endothelial sprouts forms new vessels in a tissue analogue of angiogenesis. *Integr. Biol. (Camb)*. **4**, 857–62 (2012).
77. G. M. Whitesides, A. D. Stroock, Flexible methods for microfluidics. *Phys. Today*. **54**, 42–48 (2001).
78. D. C. Duffy, J. C. McDonald, O. J. Schueller, G. M. Whitesides, Rapid Prototyping of Microfluidic Systems in Poly(dimethylsiloxane). *Anal. Chem.* **70**, 4974–84 (1998).
79. X. Chen *et al.*, Prevascularization of a fibrin-based tissue construct accelerates the formation of functional anastomosis with host vasculature. *Tissue Eng. Part A*. **15**, 1363–71 (2009).
80. C. M. Ghajar, K. S. Blevins, C. C. W. Hughes, S. C. George, A. J. Putnam, Mesenchymal stem cells enhance angiogenesis in mechanically viable prevascularized tissues via early matrix metalloproteinase upregulation. *Tissue Eng.* **12**, 2875–88 (2006).
81. X. Chen *et al.*, Rapid anastomosis of endothelial progenitor cell-derived vessels with host vasculature is promoted by a high density of cotransplanted fibroblasts. *Tissue Eng. Part A*. **16**, 585–94 (2010).
82. Y.-C. Tung *et al.*, High-throughput 3D spheroid culture and drug testing using a 384 hanging drop array. *Analyst*. **136**, 473–8 (2011).
83. B. Weigelt, A. T. Lo, C. C. Park, J. W. Gray, M. J. Bissell, HER2 signaling pathway activation and response of breast cancer cells to HER2-targeting agents is dependent strongly on the 3D microenvironment. *Breast Cancer Res. Treat.* **122**, 35–43 (2010).
84. K. M. Yamada, E. Cukierman, Modeling tissue morphogenesis and cancer in 3D. *Cell*. **130**, 601–10 (2007).

85. G. Chen *et al.*, Matrix mechanics and fluid shear stress control stem cells fate in three dimensional microenvironment. *Curr. Stem Cell Res. Ther.* **8**, 313–23 (2013).
86. U. S. Schwarz, M. L. Gardel, United we stand: integrating the actin cytoskeleton and cell-matrix adhesions in cellular mechanotransduction. *J. Cell Sci.* **125**, 3051–60 (2012).
87. T. W. Kragstrup, M. Kjaer, A. L. Mackey, Structural, biochemical, cellular, and functional changes in skeletal muscle extracellular matrix with aging. *Scand. J. Med. Sci. Sports.* **21**, 749–57 (2011).
88. D. Ribatti, B. Nico, E. Crivellato, The role of pericytes in angiogenesis. *Int. J. Dev. Biol.* **55**, 261–8 (2011).
89. N. Takakura, Role of intimate interactions between endothelial cells and the surrounding accessory cells in the maturation of blood vessels. *J. Thromb. Haemost.* **9 Suppl 1**, 144–50 (2011).
90. P. C. Stapor, R. S. Sweat, D. C. Dashti, A. M. Betancourt, W. L. Murfee, Pericyte dynamics during angiogenesis: new insights from new identities. *J. Vasc. Res.* **51**, 163–74 (2014).
91. C. L. E. Helm, A. Zisch, M. A. Swartz, Engineered blood and lymphatic capillaries in 3-D VEGF-fibrin-collagen matrices with interstitial flow. *Biotechnol. Bioeng.* **96**, 167–176 (2007).
92. C.-L. E. Helm, M. E. Fleury, A. H. Zisch, F. Boschetti, M. A. Swartz, Synergy between interstitial flow and VEGF directs capillary morphogenesis in vitro through a gradient amplification mechanism. *Proc. Natl. Acad. Sci. U. S. A.* **102**, 15779–15784 (2005).
93. C. P. Ng, C. L. E. Helm, M. A. Swartz, Interstitial flow differentially stimulates blood and lymphatic endothelial cell morphogenesis in vitro. *Microvasc. Res.* **68**, 258–264 (2004).
94. M. A. Swartz, M. E. Fleury, Interstitial flow and its effects in soft tissues. *Annu. Rev. Biomed. Eng.* **9**, 229–56 (2007).
95. S. Goel *et al.*, Normalization of the vasculature for treatment of cancer and other diseases. *Physiol. Rev.* **91**, 1071–1121 (2011).
96. J. R. Less, M. C. Posner, T. C. Skalak, N. Wolmark, R. K. Jain, Geometric resistance and microvascular network architecture of human colorectal carcinoma. *Microcirculation.* **4**, 25–33 (1997).

97. J. R. Less, T. C. Skalak, E. M. Sevick, R. K. Jain, Microvascular architecture in a mammary carcinoma: Branching patterns and vessel dimensions. *Cancer Res.* **51**, 265–273 (1991).
98. S. BOYDEN, The chemotactic effect of mixtures of antibody and antigen on polymorphonuclear leucocytes. *J. Exp. Med.* **115**, 453–466 (1962).
99. J. D. Shields *et al.*, Autologous chemotaxis as a mechanism of tumor cell homing to lymphatics via interstitial flow and autocrine CCR7 signaling. *Cancer Cell.* **11**, 526–38 (2007).
100. U. Haessler, J. C. M. Teo, D. Foretay, P. Renaud, M. A. Swartz, Migration dynamics of breast cancer cells in a tunable 3D interstitial flow chamber. *Integr. Biol. (Camb).* **4**, 401–9 (2012).
101. C. Bonvin, J. Overney, A. C. Shieh, J. B. Dixon, M. A. Swartz, A multichamber fluidic device for 3D cultures under interstitial flow with live imaging: development, characterization, and applications. *Biotechnol. Bioeng.* **105**, 982–91 (2010).
102. E. Zudaire, L. Gambardella, C. Kurcz, S. Vermeren, A computational tool for quantitative analysis of vascular networks. *PLoS One.* **6** (2011), doi:10.1371/journal.pone.0027385.
103. H. Cho, H. Y. Kim, J. Y. Kang, T. S. Kim, How the capillary burst microvalve works. *J. Colloid Interface Sci.* **306**, 379–385 (2007).
104. S. H. Zigmond, Ability of polymorphonuclear leukocytes to orient in gradients of chemotactic factors. *J. Cell Biol.* **75**, 606–616 (1977).
105. R. K. Jain, R. J. Stock, S. R. Chary, M. Rueter, Convection and diffusion measurements using fluorescence recovery after photobleaching and video image analysis: in vitro calibration and assessment. *Microvasc. Res.* **39**, 77–93 (1990).
106. A. Khademhosseini *et al.*, Co-culture of human embryonic stem cells with murine embryonic fibroblasts on microwell-patterned substrates. *Biomaterials.* **27**, 5968–77 (2006).
107. S. Valastyan, R. A. Weinberg, Tumor metastasis: molecular insights and evolving paradigms. *Cell.* **147**, 275–92 (2011).
108. P. S. Steeg, Tumor metastasis: mechanistic insights and clinical challenges. *Nat. Med.* **12**, 895–904 (2006).
109. Y. Zhang, S. Neelamegham, An analysis tool to quantify the efficiency of cell tethering and firm-adhesion in the parallel-plate flow chamber. *J. Immunol. Methods.* **278**, 305–17 (2003).

110. P. Friedl, J. Locker, E. Sahai, J. E. Segall, Classifying collective cancer cell invasion. *Nat. Cell Biol.* **14**, 777–83 (2012).
111. P. B. Armstrong, J. P. Quigley, E. Sidebottom, Transepithelial invasion and intramesenchymal infiltration of the chick embryo chorioallantois by tumor cell lines. *Cancer Res.* **42**, 1826–1837 (1982).
112. A. B. Al-Mehdi *et al.*, Intravascular origin of metastasis from the proliferation of endothelium-attached tumor cells: a new model for metastasis. *Nat. Med.* **6**, 100–2 (2000).
113. K. J. Luzzi *et al.*, Multistep nature of metastatic inefficiency: dormancy of solitary cells after successful extravasation and limited survival of early micrometastases. *Am. J. Pathol.* **153**, 865–73 (1998).
114. K. Stoletov *et al.*, Visualizing extravasation dynamics of metastatic tumor cells. *J. Cell Sci.* **123**, 2332–41 (2010).
115. C. P. Huang *et al.*, Engineering microscale cellular niches for three-dimensional multicellular co-cultures. *Lab Chip.* **9**, 1740–8 (2009).
116. S. Bersini, J. S. Jeon, M. Moretti, R. D. Kamm, In vitro models of the metastatic cascade: from local invasion to extravasation. *Drug Discov. Today.* **19**, 735–742 (2014).
117. J. M. Chan *et al.*, Engineering of in vitro 3D capillary beds by self-directed angiogenic sprouting. *PLoS One.* **7**, e50582 (2012).
118. G. M. Whitesides, E. Ostuni, S. Takayama, X. Jiang, D. E. Ingber, Soft lithography in biology and biochemistry. *Annu. Rev. Biomed. Eng.* **3**, 335–73 (2001).
119. J. Lee, M. J. Cuddihy, N. A. Kotov, Three-dimensional cell culture matrices: state of the art. *Tissue Eng. Part B. Rev.* **14**, 61–86 (2008).
120. K. E. Sung, D. J. Beebe, Microfluidic 3D models of cancer. *Adv. Drug Deliv. Rev.* (2014), doi:10.1016/j.addr.2014.07.002.
121. L. Wang, B. Sun, K. S. Ziemer, G. A. Barabino, R. L. Carrier, Chemical and physical modifications to poly(dimethylsiloxane) surfaces affect adhesion of Caco-2 cells. *J. Biomed. Mater. Res. A.* **93**, 1260–71 (2010).
122. G. K. Toworfe, R. J. Composto, C. S. Adams, I. M. Shapiro, P. Ducheyne, Fibronectin adsorption on surface-activated poly(dimethylsiloxane) and its effect on cellular function. *J. Biomed. Mater. Res. A.* **71**, 449–61 (2004).
123. M. W. Toepke, D. J. Beebe, PDMS absorption of small molecules and consequences in microfluidic applications. *Lab Chip.* **6**, 1484–6 (2006).

124. B. Huang, H. Wu, S. Kim, R. N. Zare, Coating of poly(dimethylsiloxane) with n-dodecyl-beta-D-maltoside to minimize nonspecific protein adsorption. *Lab Chip*. **5**, 1005–7 (2005).
125. I. J. Fidler, The pathogenesis of cancer metastasis: the “seed and soil” hypothesis revisited. *Nat. Rev. Cancer*. **3**, 453–8 (2003).
126. J. D. Crissman, J. S. Hatfield, D. G. Menter, B. Sloane, K. V Honn, Morphological study of the interaction of intravascular tumor cells with endothelial cells and subendothelial matrix. *Cancer Res*. **48**, 4065–72 (1988).
127. S. Koop *et al.*, Overexpression of metalloproteinase inhibitor in B16F10 cells does not affect extravasation but reduces tumor growth. *Cancer Res*. **54**, 4791–7 (1994).
128. Neoplastic Diseases: A Treatise on Tumours. By James Ewing, A.M., M.D., Sc.D., Professor of Pathology at Cornell University Medical College, N.Y.; Pathologist to the Memorial Hospital. Third edition. Royal 8vo. Pp. 1127, with 546 illustrations. 1928. *Phil. Br. J. Surg.* **16**, 174–175 (1928).
129. C. T. Mierke *et al.*, Breakdown of the endothelial barrier function in tumor cell transmigration. *Biophys. J.* **94**, 2832–46 (2008).
130. M. B. Chen, J. A. Whisler, J. S. Jeon, R. D. Kamm, Mechanisms of tumor cell extravasation in an in vitro microvascular network platform. *Integr. Biol. (Camb)*. **5**, 1262–71 (2013).